Modeling the Ignition of Soft Furnishings by a Cigarette

3

U.S. Department of Commerce

Technology Administration

National Institute of

Standards and Technology

August 1993

NIST Special Publication 852

NIST

Fire Safe Cigarette Act of 1990

Under the Cigarette Safety Act of 1984 (P.L. 98-567), the Technical Study Group on Cigarette and Little Cigar Fire Safety (TSG) found that it is technically feasible and may be commercially feasible to develop a cigarette that will have a significantly reduced propensity to ignite furniture and mattresses. Furthermore, they found that the overall impact of such a cigarette on other aspects of the United States society and economy may be minimal.

Recognizing that cigarette-ignited fires continue to be the leading cause of fire deaths in the United States, the Fire Safe Cigarette Act of 1990 (P.L. 101-352) was passed by the 101st Congress and signed into law on August 10, 1990. The Act deemed it appropriate for the U.S. Consumer Product Safety Commission to complete the research recommended by the TSG and provide, by August 10, 1993, an assessment of the practicality of a cigarette fire safety performance standard.

Three particular tasks were assigned to the National Institute of Standards and Technology's Building and Fire Research Laboratory:

- develop a standard test method to determine cigarette ignition propensity,
- compile performance data for cigarettes using the standard test method, and
- conduct laboratory studies on and computer modeling of ignition physics to develop valid, user-friendly predictive capability.

Three tasks were assigned to the Consumer Product Safety Commission:

- design and implement a study to collect baseline and follow-up data about the characteristics of cigarettes, products ignited, and smokers involved in fires,
- develop information on societal costs of cigarette-ignited fires, and
- in consultation with the Secretary of Health and Human Services, develop information on changes in the toxicity of smoke and resultant health effects from cigarette prototypes.

The Act also established a Technical Advisory Group to advise and work with the two agencies.

This report is one of six describing the research performed and the results obtained. Copies of these reports may be obtained from the **U.S. Consumer Product Safety Commission, Washington, DC 20207.**

3

Modeling the Ignition of Soft Furnishings by a Cigarette

Henri E. Mitler

George N. Walton

Building and Fire Research Laboratory

National Institute of Standards and Technology

Gaithersburg, MD 20899

U.S. Department of Commerce

Ronald H. Brown, Secretary

Technology Administration

Mary L. Good, Under Secretary for Technology

National Institute of Standards and Technology

Arati Prabakhar, Director

NIST Special Publication 852

August 1993

National Institute of Standards and Technology
Special Publication 852
Natl. Inst. Stand. Technol.
Spec. Pub. 852
169 Pages (Aug. 1993)
CODEN: NSPUE2

U.S. Government Printing Office
Washington: 1993

For sale by the Superintendent of Documents
U.S. Government Printing Office
Washington, DC 20402-9325

TABLE OF CONTENTS

LIST OF TABLES

LIST OF FIGURES

Certain commercial equipment, instruments, materials, or products are identified in this paper in order to specify the experimental procedure adequately. Such identification is not intended to imply recommendation or endorsement by the National Institute of Standards and Technology, nor is it intended to imply that the materials or equipment identified are necessarily the best available for the purpose.

MODELING THE IGNITION OF SOFT FURNISHINGS BY A CIGARETTE

Henri E. Mitler and George N. Walton

ABSTRACT

This paper describes the user-friendly computer models CIGARET and SUBSTRAT. CIGARET calculates the time-dependent behavior of a cigarette smoldering quietly in the air, away from surfaces. The model incorporates diffusion and convection of gases, as well as the kinetics of char oxidation. It calculates the internal heat fluxes, as well as the internal distributions of temperature, gas velocity, and oxygen concentration. SUBSTRAT determines whether a two-layer solid (with an air gap in between), exposed to a moving heating flux such as is produced by a cigarette, will ignite. Among the processes taken into consideration are three-dimensional heat conduction in the substrate and its pyrolysis. This model has successfully simulated the thermal runaway signifying smoldering ignition of the substrate when it is exposed to a set of external heating fluxes. SUBSTRAT and CIGARET have been designed to work in tandem to simulate the most frequent cause of fatal fires: cigarette ignition of upholstered furniture and bedding. Users' guides are included.

Key words: cigarettes; cigarette model; computer model; free smolder; furniture fires; ignition; mathematical modeling; modeling; pyrolysis; simulation; smoldering; substrates

I. INTRODUCTION

Lighted tobacco products (cigars, cigarettes, pipes) continue to be the leading ignition source for fatal fires in the United States (Miller, 1991). Most of those fires are established in soft furnishings: upholstered furniture and bedding. As a result, Congress passed the Cigarette Safety Act of 1984, with a goal to determine whether less fire-prone cigarettes were technically feasible. Under that Act, NIST developed prototype mathematical models of the components of this ignition scenario. The reason for having this capability is to "test" the effects that some particular change(s) in a cigarette will have on its propensity to ignite specified upholstered furniture quickly, cheaply, and repeatedly. The result was two prototype programs, TEMPSUB (for TEMPerature of a SUBstrate) and CIG25 (Gann *et al.*, 1988, Section 5).

Subsquent legislation, the Fire Safe Cigarette Act of 1990 (P.L. 101-352), mandated completion of such research, namely to:

> "(1) develop a standard test method to develop cigarette ignition propensity,
>
> (2) compile performance data for cigarettes using the standard test method developed under paragraph (1), and

(3) conduct laboratory studies on and computer modeling of ignition physics to develop valid, "user-friendly" predictive capability."

This publication describes the research performed and the results obtained in responding to the third task. The completion of the first two tasks is described in "A Computer Model of the Smoldering Ignition of Furniture," NISTIR 4973.

In this work, the ignition process is simulated using two computer codes, which are then used in tandem. While a single code of a fully interactive cigarette and substrate is ideal, the physical and numerical complexity of the combined burning near and at ignition renders it impossible to perform such computations on the personal computers of today.

Section II describes SUBSTRAT, a model of the time-dependent heating of substrate when subjected to a moving heat source, and establishes a criterion for its ignition. As in most soft furnishings, the substrate consists of a fabric layer over padding, with a potential air gap in between.

In order to examine how changing one or more properties of the cigarette will influence its ignition propensity, it is necessary to understand its behavior when smoldering. This includes knowing how its external heat flux and burning velocity depend on its various geometrical, physical, and/or chemical properties, and how these processes are modified when the cigarette lies on the substrate. Section III describes CIGARET, a model of a burning cigarette lying on a surface such as described above, describable by SUBSTRAT. Both the physics and chemistry of tobacco pyrolysis and simultaneous heat and gas transport in the cigarette are expressed by a set of coupled, nonlinear, partial differential equations with nonlinear boundary conditions. The model produces the time-dependent distributions of temperature, oxygen concentration, gas velocity, and burning rate in a freely smoldering cigarette which has user-prescribed properties.

In Section IV, we then describe how to use the two programs to simulate a burning cigarette on a susceptible substrate. SUBSTRAT reads an input file created by CIGARET, and also produces an output file which is used by CIGARET.

II. *SUBSTRAT*, A MODEL OF A SUBSTRATE SUBJECTED TO A MOVING HEAT SOURCE

A. Introduction

Consider what is involved in developing a computer model: we must simulate the behavior of a (typical) substrate when it is subjected to a heat flux. In order to do that, the physics and chemistry of the process must first be understood. It is then expressed as a set of equations describing the behavior; these equations must then be solved, with the appropriate data and boundary conditions. The solution method is numerical, and the data input is to a computer.

This program calculates the temperature of the upholstered furniture as a function of time and position, when it is exposed to a prescribed local heating flux. The furniture is simulated as a flat, horizontal cushioned seat; that is, a cushion consisting of fabric-covered foam padding. An air gap may be inserted between the two layers. The prescribed flux can be given either by a simple Gaussian function, or *via* an input file; if it is the former, the flux can be highly peaked at a point, vary with time, and move at a constant (specified) rate over the top surface of the furniture, assumed to be horizontal. The radiative and convective heat losses from the surface are given correctly. The temperature distribution within the substrate is calculated, since the temperature history will determine whether ignition takes place. If and when the temperature at a given location accelerates to a sufficiently high value ($\approx$ 500 °C), we can say that smoldering ignition has occurred. This is generally referred to as the **ignition** temperature, which is not unique, even for a well-defined material, depending also on the magnitude of the incident heat flux. The ambient oxygen level can be set at whatever value one wishes.

There are some limitations to this program. It will not tell whether **flaming** ignition takes place. It also does not treat the case where the flux is applied in a crevice, such as is formed between the seat cushion and the seat back. The program does not take oxygen diffusion within the cushion explicitly into account; hence in certain threshold situations, where a small change in oxygen concentration determines whether ignition does or does not take place, the results are ambiguous and not to be trusted. Note that it is often difficult to obtain the needed kinetic and/or thermophysical parameters for the materials; or, when available, to know how accurate they are. Therefore this caveat must also be made: even if the program were **perfect**, its results are only as good as the input parameters which are supplied. On the other hand, it should accurately reproduce or predict **trends**.

The first task is to examine the thermal response of the cushion to a specified flux distribution. This is done in Section II.B. [The flux data from the cigarette is described in Section III.] In Section II.C, the numerical solution method is presented, and some of the physics is revisited in this (numerical) context. In Section II.D we discuss a set of experiments where a mock-up was ignited, give the measured ignition times, and give the input data required to make computer runs. The results of these runs are given and then discussed in Section II.E, validating the model to some degree. Section II.F summarizes the work. For the reader interested in a more extensive discussion of this type of modeling, see the references cited here, especially the bibliography in Gann *et al.* (1988). A copy of the program on disk may be obtained from the authors, as well as a listing of the program and the program itself.

B. IGNITION DYNAMICS

The equations describing the relevant physical processes taking place in the substrate will be written in this Section. They will mostly be written in general form to start, and then particularized to our problem. The physical phenomena included in the model are summarized in Table 1 and discussed below.

Table 1. Features of the Substrate Model

Included	Not Included
two porous layers with an air gap	oxygen diffusion
3-d heat conduction	melting and/or regression of the foam
variable (prescribed) thermophysical properties	
correct (nonlinear) boundary conditions	
endothermic (non-oxidative) pyrolysis	
exothermic (oxidative) pyrolysis	
char oxidation	
arbitrary (prescribed) moving heat source	
variable grid on a moving coordinate system	
(approximate) radiative heat transfer within the material	
impinging air flow, when wanted	

1. Surface Heat Source

The potential ignition process is initiated by external heating of the surface. Thus, it is necessary to specify the heat gains at the bounding surfaces of the cushion. The cushion is assumed to be a rectangular parallelepiped, so a Cartesian coordinate system is employed. For the top surface, we first treat the localized heat flux from the glowing tip of the cigarette or other heat source. The flux consists of two parts, one due to convection (ϕ_c) and one due to radiation (ϕ_r):

$$\phi_{in} = \phi_c + \phi_r \tag{1}$$

ϕ_{in} is the heating flux reaching the surface. For a cigarette, these fluxes are strong functions of position, since the glowing tip is only a few millimeters in extent. With this formulation, ϕ_r can be expressed in the approximate form:

$$\phi_r \sim \Omega \epsilon_{cig} \sigma T_{cig}^4 + (1-\Omega)\sigma T_a^4 \tag{2}$$

where $\Omega = \Omega(r)$ is the shape, or view, factor of the cigarette as seen by the substrate at the point r. It is only approximate in this form, because the cigarette surface temperature, T_{cig}, varies strongly with position.

The convective flux is given by

$$\phi_c(x,y,t) = h[T_{cig}(x,y,t) - T_s(x,y,t)] \tag{3}$$

where h is the heat transfer coefficient, T_s is the surface temperature of the substrate, which is explicitly shown to be a function of position and time, and where T_{cig} is the cigarette surface temperature, also a function of position and time. It is important to point out here that in the TMPSUB2 version of the substrate model, the source flux must be specified by the user; in SUBSTRAT, on the other hand, the source flux can be either specified or it can be read in by the program, from a file produced by CIGARET.

It is equally necessary to specify the heat losses. If the existence of the cigarette is neglected for the moment, so that the view factors need not be considered, then

$$\phi_{out} = h(T_s - T_a) + \epsilon\sigma T_s^4 \tag{4}$$

where the first term is the convective cooling term and the second is the radiative cooling term. In contrast to the source term, these losses are explicitly included in the program. Here, the dependence of T_s on x, y, and t has not been shown explicitly. ϵ is the emissivity of the surface and σ is the Stefan-Boltzmann constant. (Note: we have used ε where sometimes α, the **absorptivity** of the surface, should be used. When there is thermal equilibrium between the radiation field and the hot surface, then $\alpha = \varepsilon$. We have assumed the latter, for simplicity). Evidently, the loss rate from the cushion surface increases as it heats up. h is determined by the laws of fluid flow, as well as the thermal properties of air; the simplest way to find h, however, is to use well-known expressions, usually derived from correlations. This will be further discussed below.

Along with the partial differential equation (12), we must have boundary conditions: for the top surface, the net flux entering the surface at each point is connected to the net flux according to

$$\phi_{net}(x,y,t) = -\kappa\left(\frac{\partial T(x,y,z,t)}{\partial z}\right)_{z=0} \qquad z=0, \quad t>0 \tag{5}$$

where

$$\phi_{net} = \phi_{in} - \phi_{out}\,. \tag{6}$$

When the cigarette lies on the substrate, the mean convective heating flux over the heating region is given by

$$\phi_c = h_{in}(\bar{T}_{cig} - T_s) \tag{7}$$

If h_q is the heat transfer coefficient for quiescent air, then the surface heat loss for the areas away from the cigarette is

$$\phi_{out} = h_q(T_s - T_a) \tag{8}$$

The boundary condition is greatly simplified if we can say that equation (8) is valid over the entire surface. That is readily achieved by using the model convective heating flux ϕ_c^*,

$$\phi_c^* = h_{in}(\bar{T}_{cig} - T_s) + h_q(T_s - T_a) \tag{9}$$

h_{in} is found as follows: the mean initial convective flux from a cigarette was measured to be 37 kW/m^2. Taking the mean value of the cigarette surface temperature to be about $<T>_{cig} \approx 450$ °C, the mean heat transfer coefficient in this area is $h_{in} \approx (37000/430) = 86$ W/m^2 K. h_q is found from Table 7-1 of Holman (1981): the Nusselt number for a heated, horizontal, upward-facing surface is

$$Nu = 0.54(Ra)^{1/4} \tag{10}$$

where Ra is the Rayleigh number. Since $h = \kappa Nu/L$, where L is the characteristic dimension of the surface, we find:

$$h = 0.54\,\kappa\left[\frac{g\beta(T_s - T_a)}{\alpha\nu L}\right]^{1/4} \tag{11}$$

where β is the volumetric coefficient of (gas) expansion. Taking the value for $T_s = 500$ K ≈ 227 °C as an approximate mean temperature of the surface, and L = 7 mm, we find:

$$h_q = 9.7 \text{ W/m}^2\text{-K}$$

For the other surfaces, the boundary conditions (b.c.) can be expressed in different forms, depending on whether the slab for which we are making calculations is exposed to the air, or is embedded within the cushion. If the slab were the entire cushion -- that is, the other five surfaces are exposed to the air, then the b.c. would be that the heat fluxes $\kappa\partial T/\partial x$, $\kappa\partial T/\partial y$, $\kappa\partial T/\partial z$, are given by terms of exactly the same form as (4), except that h is different for the vertical and the downward-facing horizontal surface. On the other hand, the numerical calculation we are using makes using the entire cushion prohibitively large. We therefore consider a subsection abstracted from the whole cushion, and the other five faces are surrounded by more foam. If that foam were a perfectly insulating material, then the b.c. at those faces is the adiabatic condition; that is, no flux crosses the surfaces: $\kappa\partial T/\partial x = \kappa\partial T/\partial y = \kappa\partial T/\partial z = 0$. This eliminates any heat losses from the slab, and makes the calculated temperatures somewhat higher than they really are. A simpler b.c. is to assume that the temperature at the five faces is constant and unchanging, remaining at the original (usually ambient) temperature. This produces a larger temperature gradient than actually prevails, and errs in the opposite direction. That is the default b.c. used in the calculation, but which of the two b.c.'s is used is determined by an input parameter.

2. Heat Transfer

The partial differential equation which describes the conduction of heat in a solid, when there is no radiation heat transfer, does so by giving the rate of change of temperature at every point within the solid. It is (see, *e.g.*, Carslaw and Jaeger (1959))

$$\rho\frac{\partial cT}{\partial t} = \text{div}(\kappa\,\text{grad}\,T) + S \tag{12}$$

where T, which is a function of position and of time, is the variable for which we are trying to find a solution. The other symbols in this equation are: ρ is the density of the solid, c its specific heat, κ its thermal conductivity, and S is any volumetric heat source or sink. ρ, c, κ, and S may vary with position and with T. Because these may vary in equation (12), it is conceptually simple to consider a substrate which consists of layers of material. Indeed, it will be straightforward to implement this in practice, as well. Note that because we only have derivatives of T, T need not be the absolute temperature: it may be taken to be that relative to a convenient reference temperature. In other places, such as in equation (2), it must be taken to be absolute (*i.e.*, in Kelvins).

The first term on the right-hand side describes the diffusion of heat in the solid. If there is any release of heat -- usually by combustion -- at the (interior) point in question, it is given by S(x,y,z,t). A general expression for S is

$$S = \sum_i R_i H_{ci} + L_v \frac{\partial \rho}{\partial t} \tag{13}$$

where R_i is the reaction rate (in kg/m^3-s) and H_{ci} is the heat of combustion (in J/kg), for the ith reaction. If there is endothermic pyrolysis or evaporation, we have the last term on the right-hand side as well, where L_v is the latent heat of evaporation or pyrolysis. An explicit expression for R_i will be given in Section II.B.4.

Since the furniture (apart from the frame) consists of a fabric-covered pad, it is clear that the program must take at least two layers (with different properties) into account. Therefore the program was written so as to permit different values for the relevant thermophysical constants ρ, c, and κ in each layer. In fact, generally there is not perfectly intimate thermal contact between the fabric covering and the padding; there is a small but sometimes significant intervening air gap. Normally, one would place a node within this gap, in order to take a third layer into account; because of the thinness of the gap, and other technical difficulties, however, a different treatment of the effect of this air gap has been devised: the gap can be represented in terms of its "thermal resistance." (See Section II.C.3.) This has been programmed and successfully tested.

In writing equation (12), we have made the simplifying assumption that the cushion is totally opaque; that is, there is no radiative transfer of heat through the cushion. If there were, the equation describing heat transfer through the solid would become still more complicated. However, the fabric and foam can each be thought of as porous, consisting of solid parts interspersed with void spaces. Then taking forward radiation transfer in those spaces, it is possible to incorporate a first approximation to (one-d) radiation transfer, as shown by Kunii (1961)

$$\kappa(T) = (1 - \Phi^{2/3})\kappa_s + \Phi^{1/3}(\kappa_g + 2h_r D_p/3) \tag{14}$$

where Φ is the void fraction, and κ_s and κ_g are the solid and gas-phase thermal conductivities, respectively; they are each functions of T. D_p is the mean pore diameter, and

$$h_r = 4\epsilon\sigma T^3 \tag{15}$$

Equation (14) was equation (5-50) in Gann *et al.* (1988). Finally, we must note that at a given temperature, the thermal conductivity is proportional to the density (also see Section II.C.5):

$$\kappa(\rho) = (\rho/\rho_a)\kappa(\rho_a) \tag{16}$$

3. Time to Ignition

An experimental test for the time to ignition is described in Section II.D. We can readily make an order-of-magnitude estimate for this time, based on equation (12). For the very special case that the substrate is initially at the uniform temperature T_o, that it is homogeneous, isotropic, inert, and semi-infinite, that the thermophysical characteristics ρ, c, and κ of the material are independent of the temperature, and that the problem is one-dimensional (*i.e.*, the incident flux is the same everywhere on the plane z = 0, resulting in the slab being subjected to the uniform net heating flux $\phi_{net}(t)$), then equation (12) can be solved analytically and explicitly, and it can be shown (Carslaw and Jaeger, 1959, p.76) that the surface temperature is given by

$$T_s(t) = T_o + \frac{1}{\sqrt{\pi\kappa\rho c}} \int_0^t \frac{\phi_{net}(t')\,dt'}{\sqrt{t-t'}} \tag{17}$$

For the still simpler (unrealistic) case ϕ_{net} = constant, this can be immediately integrated, and we obtain

$$T(t) = T_o + \frac{2\phi_{net}\sqrt{t}}{\sqrt{\pi\kappa\rho c}} \tag{18}$$

When the left-hand side reaches the ignition temperature T_{ig}, the time elapsed must be the time in the right-hand side of the equation, and may be called the ignition time:

$$t_{ig} = \frac{\pi\kappa\rho c}{4}\left(\frac{T_{ig}-T_o}{\phi_{net}}\right)^2 \tag{19}$$

Although not a single one of the simplifying assumptions required to obtain equation (19) is valid, this expression is nevertheless very useful as a guide to the form of the dependence of t_{ig}. In particular, we will use equation (19) in order to make sense out of the experimental observations, in Section II.E.1.

[We can, at some cost in computation time, get a somewhat more realistic result by relaxing one of the assumptions above: it is possible to write, starting with equation (17), an explicit expression for $T_s(t)$ for the case where the net flux is not constant, but results from some impressed external flux, diminished by a Newtonian (*i.e.*, linear) cooling loss; that is, where we can write $\phi_{loss} = h^*(T_s - T_s)$; see Quintiere (1988)].

4. Pyrolysis of the Substrate

As described above, we assume that the substrate consists of a thin fabric covering a relatively thick foam pad, with a very thin air gap between them. Each of the two materials will be heated and can pyrolyze. In this Section we describe how these reactions are calculated. Pyrolytic reactions can generally be expressed in the Arrhenius form

$$R_p(T, \rho_f, \rho_o) = A\,\rho_f^m\,\rho_{ox}^n\,e^{-E_A/RT} \qquad \text{kg/m}^3\cdot\text{s} \tag{20}$$

where ρ_f is the density of the fuel and ρ_{ox} that of oxygen; E_A is the activation energy for the reaction, and R is the universal gas constant (not to be confused with the reaction rate R_p in equation (20)). It is sometimes convenient to define an "activation temperature" T_A:

$$T_A \equiv E_A/R \tag{21}$$

In the remainder of the paper, R is used only to represent a reaction rate. All the quantities in equation (20) except the pre-exponential factor A are at the location (x,y,z) within the porous solid and at the time t; this dependence is not shown explicitly in order to minimize the complexity of the expression. Similarly, the subscript i, corresponding to ith "reaction" has been suppressed from R, A, ρ_f, m, n, and E_A. If the reactions were truly elemental Arrhenius reactions, then m = n = 1. However, equation (20) is really a model equation, and therefore m and n are purely empirical parameters (just as A and E_A are), and need not be integers.

Oxidative as well as non-oxidative pyrolysis (thermal decomposition) of materials have been included. The former reactions are generally exothermic, while the latter are generally endothermic. There may be several oxidative reactions as well as several non-oxidative ones; char oxidation, when it takes place, is the last step. In this model a maximum of three reactions is permitted for each material. The oxidative reactions are exothermic; we assume that the rate of each step (reaction) is adequately described by an Arrhenius equation of the form (20).

It had been hoped that the different pyrolysis steps take place at sufficiently different temperatures, that the reaction sequence for the ignition of the fabric could be taken to consist of a small number of steps which follow each other sequentially. That would correspond to the equations taking the form

$$R_p = \sum_i R_{pi} = \sum_i A_i (\rho - \rho_i)^{n_i} \rho_{ox}^{n_i} \exp(-T_i/T) \tag{22}$$

where ρ_i is the density of the fuel at the end of the i^{th} reaction step. When the reaction produces a gaseous species which escapes, the reaction rate is given by

$$R_p = -\frac{\partial \rho}{\partial t} \tag{23}$$

More generally, if species i is reacting and producing species j, then

$$\frac{\partial \rho_i}{\partial t} = -R_i = -\frac{\partial \rho_j}{\partial t} \tag{24}$$

We will here discuss only the pyrolysis of the fabric, which is of principal interest: when smoldering ignition is produced, it is almost always first initiated in the fabric. Pyrolysis of the foam is discussed briefly in Section II.D.2. The fabric of particular interest is cotton duck; cotton is principally cellulose.

Analysis of the reaction kinetics of a cellulosic paper by Kashiwagi and Nambu (1992) showed that it could be described by three reactions, all of which will proceed simultaneously (though obviously at different rates). That means that the equations describing the creation and destruction of different fuel species must be included. Virgin material goes to char, *via* two pathways: degradation and oxidative pyrolysis. Each gram produces n_c grams of char. The char then goes to ash, *via* char oxidation. Each gram of char produces n_a grams of ash. Thus one gram of material produces $n_a n_c$ grams of ash. The governing equations are

$$\dot{\rho}_v = -R_d - R_{op} \tag{25a}$$

$$\dot{\rho}_c = n_c(R_d + R_{op}) - R_{co} \tag{25b}$$

and

$$\dot{\rho}_a = n_a R_{co} \tag{25c}$$

The density of the solids is

$$\rho_s = \rho_v + \rho_c + \rho_a \tag{25d}$$

Hence

$$\dot{\rho}_s = -(1 - n_c)(R_d + R_{op}) - (1 - n_a)R_{co} \tag{25e}$$

The subscripts denote:

a = ash	op = oxidative pyrolysis
c = char	s = solid
co = char oxidation	v = virgin material
d = degradation	

Besides the surface heat source described in Section II.B.1, there are also internal heat sources (and sinks), given by equation (13). The heats of combustion must be supplied by the user of the model; those for cotton are given in Section II.D. The global kinetic constants given by Kashiwagi and Nambu are also listed in Section II.D. If the reaction rate of one or more exothermic reactions becomes high, for any reason, the rate at which energy is being generated will exceed the rate at which it is lost, and a "thermal runaway" will ensue, very similar to a chain reaction. During the runaway, the rate of pyrolysis (and of heating) is limited by the availability of oxygen. Since O_2 has 0.001 times the density of the local fuel, it would immediately be exhausted, but for the supply which (a) diffuses in from adjoining cells, and that which (b) diffuses in (or is convected in) from the surface.

5. Gas Diffusion

As oxygen is depleted in the regions where combustion (oxidative pyrolysis, char oxidation) is taking place, the concentration gradient which results will induce diffusion of oxygen into those regions, from the surface as well as from adjacent, oxygen-rich regions, assuming the medium is porous and permits diffusion. Similarly, the gaseous (and other) products which are generated -- mainly CO_2 -- build up in local concentration, and diffuse away.

The equations which describe the rate of change of species concentration are analogous to equation (12) for the diffusion of heat; assuming no convection, the ith species density is governed by

$$\frac{\partial \rho_i}{\partial t} = \text{div}(D_{io}\,\text{grad}\,\rho_i) + S_i \tag{26}$$

where D_{io} is the diffusion coefficient for species i in the background "o," and S_i is the source/sink term. If the diffusion coefficient increases with T, as it normally does, then the CO_2 diffusion, for example, will take place preferentially towards the hot regions, *i.e.*, towards the surface. The migration of gases is expected to have a minor effect on the heat transfer, and hence on the temperature distribution, from

this effect. However, the diffusion of oxygen is important: the rate at which oxygen enters the reacting region sets the limit on the reaction rate.

A porous medium is one consisting of solid particles embedded in a gaseous medium. Put in a different way, a gas molecule cannot penetrate any of the solid phase, but is able to traverse the entire medium, either because of a pressure difference, or merely from the "random walk" which constitutes diffusion. The diffusivity of a gas species in such a medium is really the diffusivity of those gas molecules through a gaseous medium consisting of the same or some other gas, where the solid volumes are excluded. That is the **effective** diffusivity.

It has been found experimentally (Szekely *et al.*, 1976) that, approximately,

$$D_{eff} = D_o \Phi^n \tag{27}$$

where Φ is the fractional void space; this is also referred to as the "porosity" in the literature. The relationship is strongly dependent on the structure of the (granular) material; thus, Figure 2.4 from Szekely *et al.*, 1976, shows that for particles of mica,

$$D_{eff} / D_o = \Phi^{10.3} \tag{27a}$$

whereas for sand, a bed of glass spheres, carborundum powder, and table salt,

$$D_{eff} / D_o = 0.677\, \Phi^{1.18} \tag{27b}$$

for $\Phi < 0.7$. As shown in Appendix E, $\Phi \approx 0.6$ for the cotton fabric that will be our main focus of interest; hence equation (27b) is the relationship to be used.

Here D_o is the diffusivity of O_2 in N_2. From equation (16.3-1) of Bird *et al.* (1960), we find that for O_2 in N_2, the temperature dependence is

$$D_o(T) = 0.199 \left(\frac{T}{293.16} \right)^{1.823} \qquad \text{cm}^2/\text{s} \tag{28}$$

6. Boundary Conditions for Gases

There are two cases of interest: first, when the air above the substrate is quiescent, and second, when -- as was the case in the experiment to be described in Section II.D -- there is a stream of air impinging on the substrate. We first obtain a general expression:

When the air above the substrate is quiescent, and there are oxidative reactions taking place in the substrate, the concentration of oxygen molecules in the air decreases towards the surface, through a boundary layer. The maximum possible reaction rate is obtained by assuming $y_s = 0$, as can be seen from equation (29). On the other hand, this is clearly not possible, since we must have a finite concentration at the surface in order to get any reactions at all. It is possible to obtain a value for y_s analytically, if one makes the simplifying assumptions of an isothermal substrate and a first-order reaction rate (Ohlemiller, 1991).

Mass transfer is a (molecular) transport phenomenon, just as is heat (momentum) transfer. Thus, analogous to the first term on the right-hand side of equation (4), the mass transfer of oxygen across the surface of the solid can be written as

$$\dot{m}''_{O2}(x,y) = k_{gas}[Y_a - Y_s(x,y)] \tag{29}$$

where Y_a is the ambient oxygen mass fraction and Y_s that at the solid surface; the x,y dependence of the latter has been put in explicitly in order to emphasize the origin of the spatial dependence of $\dot{m}_{O2}''$. This is the boundary condition.

Note: The **velocity** at which oxygen enters the surface is

$$V_o = D\left(\frac{\partial Y}{\partial x}\right)_s = \gamma(Y_a - Y_i) \tag{30}$$

(see Gann *et al.*, 1988, pp. 159-160) where D is the diffusion coefficient inside the solid. Thus

$$k_{gas} = \rho_a \gamma \tag{31}$$

where γ is the normalized mass transfer coefficient for oxygen traversing the boundary layer above the substrate. In SUBSTRAT (see Gann *et al.* (1988), equation (5-64) (from Muramatsu, 1981)), the following equation was used for γ:

$$\gamma_b = 6.38x10^{-3}\left[\frac{T^{2.75}(T - T_a)(T + 123.6)}{RT_a}\right]^{1/4} \quad \text{cm/s} \tag{32}$$

where the subscript "b" refers to "boundary layer". On the other hand, in this paper we obtain γ in a different way; we will afterwards use equation (32) in order to compare the results. The way γ is obtained is as follows: Because of the similar origin of mass and heat transfer, one can often use the Reynolds-Colburn analogy. It is not difficult to show, from the treatment in Chapter 3 of Treybal (1955), that the Reynolds-Colburn analogy leads to

$$\gamma = \frac{h\,Pr^{2/3}}{\rho\, c_p\, Sc^{2/3}} \quad \text{m/s} \tag{33}$$

where h is the heat transfer coefficient appropriate to the problem, Pr is the Prandtl number, Sc is the Schmidt number (Sc = ν/D), and ν is the kinematic viscosity. Once we have γ_b, equation (31) gives k_{gas}, to be used in equation (29).

Case A. Quiescent air

Here we have

$$h = \kappa Nu/l_c \tag{34}$$

where κ is the thermal conductivity, l_c is a characteristic dimension for the problem, and Nu is the Nusselt number. We can thus rewrite equation (33) as

$$\gamma = \frac{\alpha}{l_c} Nu \left(\frac{Pr}{Sc}\right)^{2/3} \tag{35}$$

In quiescent air, there is a constant movement of molecules in all directions; the flow in any one direction is exactly compensated by the flow in the opposite direction, normally. If, however, the gas is near a boundary which "absorbs" some of these molecules (as is the case for oxygen impinging on a reactive substrate) then evidently the return flow is smaller, and hence the impinging flow is not completely nullified. The result is that there is a gradual decrease in the concentration of those molecules as the surface is approached. This region is referred to as the "boundary layer."

The quantities in equation (35) are to be evaluated at some characteristic (mean) temperature of the boundary layer. That temperature can be taken to be the mean between T_a and T_s. For quiescent air, with the surface horizontal and facing upward, l_c is the boundary layer thickness. The expression for the Nusselt number is given in Section II.B.1.

Case B. Impinging Air

The Nusselt number for this case is given by equation (D10), Appendix D. Inserting that into equation (35), we obtain

$$\gamma = 0.767 \frac{\alpha}{l_c} \sqrt{Re}\, Pr^{1.07} Sc^{-2/3} \tag{36}$$

where α is the thermal diffusivity of air, $Re = u_o l_c/\nu$ is the Reynolds number and u_o is the incoming velocity of the impinging flow.

We now show that when oxygen consumption is significant, it takes place in a very narrow layer; this is analogous to the flame sheet approximation for combustion in air. As a result, we may take the concentration of oxygen in that layer to be some appropriate average value, rather than having to actually program in the species diffusion equations, *via* equation (26).

7. Oxygen Diffusion

In this Section, it is shown that a reasonable approximation to the overall reaction rate can be obtained without explicitly solving the gas diffusion equation, equation (26), for the diffusion of oxygen in the substrate. This is the approximation made in the model.

In the experiment to be discussed in Section II.D, a jet of air is directed downward at the substrate. Hence there is no boundary layer in this case, and the oxygen concentration just outside the surface is 21%. When the reaction rate is low, the oxygen concentration in the top of the substrate will not be much affected by the slow reactions. When the reaction rate becomes high, on the other hand, the mean oxygen concentration in that thin layer becomes low. It cannot get too low, however, since (as discussed in Section II.B.6), the reaction rate would then fall. Hence a quasi-steady state is established. Thus, in the "runaway" phase, the reaction rate must be given by the boundary condition equation (29).

We will now argue that when significant oxidative pyrolysis is taking place,

(a) taking a constant value for the oxygen concentration ($[O_2]$) in the substrate is a valid approximation,

(b) most of the pyrolysis occurs in the surface layer, and therefore

(c) we obtain an adequate approximation to the pyrolysis rate, without explicitly including the oxygen diffusion equations.

When the surface temperature is relatively low, there is negligible pyrolysis, and the oxygen distribution $[O_2](x)$ in the substrate is approximately uniform. When T_s has risen to the point that perceptible pyrolysis is taking place at and near the surface, the $[O_2]$ profile in the substrate dips as the surface is approached from below (*i.e.*, from within);it must reach a minimum and then rise again at the surface, because of the diffusion of oxygen from outside. When the temperature reaches values so high that $[O_2]$ is pulled down to negligible values near (but not at) the surface, the principal source of oxygen in the reaction zone is from the air diffusing in from the surface; the region where there is significant oxidative reaction is then highly localized near the surface, with $[O_2]$ being highest at the surface, and falling rapidly until it reaches negligible values. The characteristic oxygen penetration distance is δ, and it is clear that δ is a steeply falling function of T. [At some further distance in, the oxygen must diffuse towards the surface from other (deeper, or peripheral) parts of the porous substrate, because of the concentration gradient, so that the profile must rise again as we go deeper. It can do so because at that depth the temperature has fallen sufficiently to "freeze out" the (oxidative) reaction rate, *i.e.*, it is negligibly small].

Suppose that T_s is high enough to drive $[O_2]$ to near-zero at some depth. Then we may write, crudely,

$$Y(x) \sim Y_s e^{-x^2/\delta^2} \tag{37}$$

with Y_s = surface value of $[O_2]$, and δ = characteristic penetration depth. If we write the reaction rate in the form

$$R[x,T(x)] = Y(x)^n F[x,T(x)] \equiv Y^n G(x) \tag{38}$$

then the total reaction rate per unit area is

$$\dot{m}'' = \int_o^\infty Y(x)^n G(x)\, dx \tag{39}$$

where G(x) is a fairly steep (decreasing) function of x. We may thus further write (still very crudely)

$$G(x) \sim G_o e^{-x^2/\theta^2} \tag{40}$$

Then

$$\dot{m}'' \sim \int_o^\infty Y_s^n e^{nx^2/\delta^2} G_0 e^{-x^2/\theta^2}\, dx = G_0 Y_s^n \frac{\sqrt{\pi}}{2}\left(\frac{1}{\theta^2} + \frac{n}{\delta^2}\right)^{-1/2} \tag{41}$$

We use the mean-value theorem, and write the integral in equation (41) as

$$\int_o^\infty \bar{Y}^n G_o e^{-x^2/\theta^2}\, dx = \bar{Y}^n G_o \theta\sqrt{\pi}/2 \tag{42}$$

Then

$$\bar{Y}^n = Y_s^n \left(1 + \frac{n\theta^2}{\delta^2}\right)^{-1/2} \tag{43}$$

We now need an estimate for θ/δ. Clearly, the reaction rate must be significant for a distance comparable to the penetration depth δ: else, if the reactions "froze" before $[O_2]$ becomes negligible, $[O_2]$ would not fall below some appreciable value. Moreover, the reaction rate cannot be significant below that depth, precisely because there is so little oxygen below. Thus $\theta \approx \delta$. For n, we take $n_o = 0.5$, as given in Kashiwagi and Nambu (1992). Then equation (43) yields

$$\bar{Y} = 2Y_s/3 \tag{44}$$

Next, consider the effect of discretizing the equations (Section II.C). If $\delta > \Delta x$, then assuming that the reaction takes place in the top cells only, clearly underestimates the reaction rate. However, when δ is large, the total reaction rate is very low. That is, while the fractional error is large, the absolute error is small, and (we shall show) typically negligible.

Assume, for the sake of simplicity, only one oxidation reaction. Assume, also, that the temperature and reaction rate are uniform in a thin sheet of depth δ at the surface, where T is maximum. (This is essentially what is implicitly assumed in the numerical calculation.) Then if the stoichiometric fuel/oxygen ratio is r, the fuel burnup rate is

$$R\delta = \dot{m}_f'' = r\,\dot{m}_{ox}'' \tag{45}$$

where R is the reaction rate (g/cm^3s or kg/m^3s). If δ is greater than the thickness of the surface cell, then evidently the reaction rate in the top layer is limited to $R\Delta z$; whereas if $\delta < \Delta z$, equation (45) gives the limit. Thus the reaction rate in the top cell is

$$R_{top}\Delta z = \min[R\Delta z,\ r\,\dot{m}_{ox}''] \quad g/cm^2\text{-}s \tag{46}$$

Note that when the reaction rate is so high that $\delta < \Delta z$, the concentration at the bottom face of the top cell(s) is close to zero; therefore a reasonable value to take for $[O_2]$ in the cell is on the order of the mean value, 11%, (or 0.12 for the mass fraction); or, according to equation (44), $<Y> \approx \frac{2}{3}(0.2318) = 0.15$.

We now make a calculation to find a typical value for δ. As is clear from equation (45), we must begin by calculating a reaction rate R. In order to find R, we must anticipate some results from Section II.D.2. Using equations (79) and (80), we find that

$$R_{op} = \rho_v k_{op} = \rho_v\ 1.5\text{x}10^{14}\ Y^{0.5}\ (W_d/W_o)^{1.3}\ \exp(-160/RT)$$

and

$$R_{co} = \rho_c k_{co} = \rho_c\ 3.4\text{x}10^{11}\ Y^{0.78}\ (W_c/W_o)\ \exp(-160/RT)$$

The meaning of the subscripts is made clear in the list below equation (25e). These rates are in kg/m^3 min. We must choose characteristic values for ρ_v, Y, W_d/W_o, ρ_c, W_c/W_o, and T, in order to get estimates. Reasonable values are:

$$W_d = W_o/2,\ W_c = W_o/4,\ \text{and}\ Y \approx 0.11$$

For ρ_v and ρ_c, we assume that the volumes are unchanged, so that

$$\rho_v/\rho_o = W_d/W_o \quad \text{and} \quad \rho_c/\rho_o = W_c/W_o$$

Finally, we take $\rho_o = 1560$ kg/m^3. We then find that

$$k_{op} = 2.02\text{x}10^{13} \exp(-160/RT) \ \text{min}^{-1}$$

and

$$k_{co} = 1.52\text{x}10^{10} \exp(-160/RT) \ \text{min}^{-1}$$

The universal gas constant R = 8.31447 J/mol-K, so that the activation temperature for both reactions is

$$T_A = 160{,}000/R = 19244 \text{ K.}$$

For a temperature in the vicinity of the ignition temperature, say, 400 °C = 673.16 K, we then have

$$k_{op} = 7.77 \text{ min}^{-1} \quad \text{and} \quad k_{co} = 0.00584 \text{ min}^{-1},$$

yielding

$$R_{op} = \rho_v k_{op} = 101 \text{ kg/m}^3 \text{ s}$$

and

$$R_{co} = \rho_c k_{co} = 0.038 \text{ kg/m}^3 \text{ s.}$$

Thus at 400 °C, with these assumptions for ρ_v and ρ_c, oxidative pyrolysis takes place more than 2600 times faster than does char oxidation, and we may therefore take

$$R = R_{op} = 101 \text{ kg/m}^3 \text{ s}$$

Next, we need to have the rate at which oxygen enters the medium, $\dot{m}''_{ox}$. Equations (29) and (31) give the required value. For the ignition experiment, the appropriate expression to use to find γ is equation (36). The temperature at which the various quantities must be evaluated is that of the purging gas. Examination of Table D-1 in Appendix D shows that T_g is quite high. Assume T_g = 800 K. Equation (28) yields $D_o(800) = 1.24$ cm^2/s. Then the Schmidt number is Sc = 0.663, and

$$\gamma \approx 8.10\text{x}10^{-5} \sqrt{\text{Re}} \, / \ell_c \ \text{m/s}$$

(with ℓ_c in meters). The characteristic air velocity for calculating Re is given by eauation (D15) in Appendix D. Finally, the characteristic length ℓ_c is the standoff distance, δ. With δ = 5.4 mm, we find Re = 11.06 and γ = 4.99 cm/s. (Incidentally, if we had quiescent air at 800 K, Muaramatsu's expression, equation (32), yields $\gamma_b \approx 2.35$ cm/s).

Finally, taking $Y_a = 0.232$ and $Y_s = 0$, equations (29) and (31) then yield

$$\dot{m}''_{ox} \approx 13.6 \text{ g/m}^2\text{s}$$

We must also have r (the stoichiometric fuel/oxygen ratio) in order to use equation (45) to get the penetration depth δ. The stoichiometric air/fuel mass ratio for wood is S = 5.78, close enough to that for cellulose. Hence r $\approx$ 0.746, and we find δ = 0.10 mm. Thus the penetration depth δ is indeed much smaller than the layer thickness Δx (which is of the order 0.5 mm).

For T_g = 300 °C, on the other hand, we find k_{op} = 0.053 min^{-1}, so that R_{op} = 1.38 kg/m^3 s. Then $\delta \approx$ 7.3 mm, several times Δx, but the resulting mass-loss rate is only 0.043 g/m^2 s, which is indeed negligible.

For the case of quiescent air above the substrate, the mean value for the oxygen concentration to be used in the top cell during the runaway, is midway between the value at the top surface (*i.e.*, at the bottom of the boundary layer), and at the bottom of the top cell (presumably, close to zero).

The only time that we cannot justifiably make the simplification that the oxygen concentration in the top layer is either that at the top surface or half (or 2/3) that value (during runaway), is when the reaction rate is intermediate between the very low values and the runaway value. This period should be relatively short, and the error introduced by these simplifications should not be large.

C. NUMERICS

In general, it is not possible to solve equation (12) analytically, in spite of the simplifying assumption of no radiation heat transfer, and even for the case S=0. That is, to write down an explicit expression which gives T in terms of the inputs. This is so, because of the nonlinear and nonuniform boundary conditions. It is therefore necessary to resort to a numerical procedure, which is that incorporated in TMPSUB2 and SUBSTRAT. Hereafter, we shall only refer to the latter, when something applies to both, as is the case here).

1. Introduction

The development of TMPSUB2 centers around the capability to simulate transient heat transfer. A one-dimensional heat conduction problem provides the simplest example to illustrate transient simulation methods. Figure 1 shows a portion of a one-dimensional conduction problem in which the material has been divided into thin layers. This example will be described by physical instead of mathematical arguments following the description given by Clausing (1969, pp.157-213).

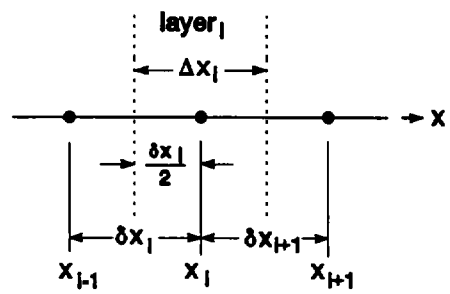

Figure 1. One-dimensional conduction

The figure focuses on a representative layer of material of thickness Δx_i centered in a node at coordinate x_i. This material layer is represented by a single temperature T_i and a corresponding thermal conductivity κ_i, density ρ_i, and specific heat c_i. Assume this layer has a surface area of magnitude A in the Y-Z plane. The distance between nodes i and i-1 is given by δx_i (= $x_i - x_{i-1}$). Subscripts i and n refer to positions in space and time, respectively. Subscript n is temporarily suppressed until it becomes necessary to consider time, in the following equations.

The instantaneous internal energy of layer i is given by

$$U_i = \rho c \Delta V T_i = \rho c \Delta x_i A T_i \equiv C_i T_i \qquad (47)$$

where T is the absolute temperature. This equation also serves to define the heat capacity, C, assigned to node i. Heat is transferred to and from layer i by three methods:

(1) conduction from layer i-1 at the rate

$$q_{i-} = (T_{i-1} - T_i)\,\kappa_{i-} A / \delta x_i = K_{i-}(T_{i-1} - T_i) \tag{48}$$

(2) conduction from layer i+1 at the rate

$$q_{i+} = (T_{i+1} - T_i)\,\kappa_{i+} A / \delta x_{i+1} = K_{i+}(T_{i+1} - T_i) \tag{49}$$

(3) internal heat generation or radiation absorbed within the layer, S_i.

Equations (48) and (49) define the thermal conductance, K, in each direction. The possibility of a thermal conductivity which varies with position is explicitly taken into account here using labels + and —: κ_{i-} and κ_{i+}. A good first order approximation for κ_{i-} is the harmonic average of κ_i and κ_{i-1}:

$$\kappa_{i-} \approx \frac{2\kappa_i \kappa_{i-1}}{\kappa_i + \kappa_{i-1}} \tag{50}$$

with a similar expression for κ_{i+}.

The change in internal energy of this layer between time t_n and time t_{n+1} is given to first order in Δt by

$$\Delta U_{i,n\to n+1} \equiv C_{i,n+1}T_{i,n+1} - C_{i,n}T_{i,n} = \Delta t\,(q_{i-} + q_{i+} + q_i) \tag{51}$$

where the time dependence has now been put in explicitly. There are several common solutions to equation (51) depending on when the heat gains are evaluated. One solution involves evaluating at time n

$$C_{i,n+1}T_{i,n+1} = C_{i,n}T_{i,n} + \Delta t\,[K_{i-}(T_{i-1,n} - T_{i,n}) + K_{i+}(T_{i+1,n} - T_{i,n}) + S_{i,n}] \tag{52}$$

which is the standard Euler explicit time integration formula. "Explicit" means that $T_{i,n+1}$ can be directly computed from values known at time n. On the other hand, evaluating at time n+1 gives

$$C_{i,n+1}T_{i,n+1} = C_{i,n}T_{i,n} + \Delta t\,[K_{i-}(T_{i-1,n+1} - T_{i,n+1}) + K_{i+}(T_{i+1,n+1} - T_{i,n+1}) + S_{i,n+1}] \tag{53}$$

which is Euler's standard implicit time integration formula. "Implicit" means that $T_{i,n+1}$ is computed from other values also evaluated at time n+1. These values depend implicitly on each other and must be computed by a solution of simultaneous equations.

Clausing (1969, p.190) also gives a discussion of stability in terms of thermodynamic laws. Rearranging equation (52) to solve for $T_{i,n+1}$ gives

$$T_{i,n+1} = (K_{i-,n}T_{i-1,n} + K_{i+,n}T_{i+1,n} + S_{i,n})\,\Delta t / C_{i,n+1} + T_{i,n}[C_{i,n} - (K_{i-,n} + K_{i+,n})\,\Delta t] / C_{i,n+1} \tag{54}$$

where the time subscript, n, has been added to the K terms to indicate exactly when these values are evaluated. For the sake of argument, assume $C_{i,n+1} = C_{i,n}$ ($=C_i$) for simplicity. There is no solution if $C_i = 0$. If C_i is sufficiently small or Δt sufficiently large, then $(K_{i-,n} + K_{i+,n})\,\Delta t / C_i > 1$, and

as $T_{i,n}$ increases $T_{i,n+1}$ must decrease, and vice versa. This is thermodynamically impossible. It shows up in a numerical solution as oscillations, *i.e.*, "instability," in the node temperatures at each time step. These oscillations tend to quickly increase to totally meaningless values. In general, the smaller the thermal mass of the element, the smaller the time step needed for a stable explicit solution. This suggests a simple technique to determine the minimum stable time step for any element in the system.

Thus, rearranging the implicit (53) to solve for $T_{i,n+1}$ gives

$$T_{i,n+1} = \frac{C_{i,n}T_{i,n} + \Delta t\,(K_{i-,n+1}T_{i-1,n+1} + K_{i+1,n+1}T_{i+1,n+1} + S_{i,n+1})}{C_{i,n+1} + \Delta t\,(K_{i-,n+1} + K_{i+,n+1})} \tag{55}$$

This equation shows none of the computational or thermodynamic problems of equation (54), indicating that the standard implicit method is stable for all time steps.

The spatial discretization error (for a uniform grid) for the standard explicit and standard implicit methods is proportional to $(\Delta x)^2$ (for a variable grid, the accuracy is reduced somewhat; see Section II.C.4). The time discretization error is proportional to Δt.

The standard explicit and standard implicit methods err in opposite directions. Therefore, a more accurate solution can be obtained by combining the two methods. Expressing this combination generally in terms of a parameter β gives

$$\Delta U_{i,n\to n+1} = \Delta t\,[(1-\beta)(q_{i-,n} + q_{i+,n} + S_{i,n}) + \beta(q_{i-,n+1} + q_{i+,n+1} + S_{i,n+1})] \tag{56}$$

where $0 \le \beta \le 1$.

$\beta = 0$ corresponds to the standard explicit method,
$\beta = 1/2$ corresponds to the Crank-Nicholson method,
$\beta = 2/3$ corresponds to the Galerkin method, and
$\beta = 1$ corresponds to the standard implicit method.

For $\beta \ge 1/2$ this method is unconditionally stable, although the solution may be oscillatory. For $\beta > 3/4$ (approximately) the solution is stable and non-oscillatory. For $\beta = 1/2$, the time discretization error is proportional to $(\Delta t)^2$.

The methods presented above extend directly into three dimensions. For a Cartesian coordinate system and a cell of dimensions Δx_i by Δy_j by Δz_k, equation (51) can be rewritten to account for conduction from the six adjacent cells in the 3-D system:

$$\Delta U_{i,j,k} = \Delta t\,(q_{i-,j,k} + q_{i+,j,k} + q_{i,j-,k} + q_{i,j+,k} + q_{i,j,k-} + q_{i,j,k+} + S_{i,j,k}) \tag{57}$$

where

$$q_{i-} = (T_{i-1,j,k} - T_{i,j,k})\,\kappa_{i-}\,\Delta y_j\,\Delta z_k / \delta x_i$$

$$q_{i+} = (T_{i+1,j,k} - T_{i,j,k})\,\kappa_{i+}\,\Delta y_j\,\Delta z_k / \delta x_{i+1}$$

$$q_{j-} = (T_{i,j-1,k} - T_{i,j,k})\,\kappa_{j-}\,\Delta x_i\,\Delta z_k / \delta y_j$$

$$q_{j+} = (T_{i,j+1,k} - T_{i,j,k})\,\kappa_{j+}\,\Delta x_i\,\Delta z_k / \delta y_{j+1}$$

$$q_{k-} = (T_{i,j,k-1} - T_{i,j,k})\,\kappa_{k-}\,\Delta x_i\,\Delta y_j / \delta z_k$$

$$q_{k+} = (T_{i,j,k+1} - T_{i,j,k})\,\kappa_{k+}\,\Delta x_i\,\Delta y_j / \delta z_{k+1}$$

and $S_{i,j,k}$ represents other heat added directly to the cell.

2. Boundary Conditions

Special treatment is required for cells on the boundaries of the region being modeled. In particular, the nodes which represent the cells are placed on the boundary, rather than at the center. Referring to the one-dimensional example in Figure 1, the surface layer is only half as thick as the others.

An adiabatic boundary condition (b.c.) is handled by setting the appropriate heat flux terms in equation (45) to zero. A constant temperature (isothermal) b.c. is handled by leaving the temperature unchanged.

The surface of the substrate (z=0 plane; see Figure 3) transfers heat to the environment by convection and by radiation. The convective heat gain for cell i,j,1 is given by

$$(S_c)_{i,j,1} = (T_a - T_{i,j,1})h\Delta x_i \Delta y_j \tag{58}$$

where T_a is the temperature of the surrounding (ambient) air, and h is the heat transfer coefficient.

A positive value of S_c represents a heat gain by the cell. The radiative heat gain is given by

$$(S_r)_{i,j,1} = \sigma\epsilon(T_a^4 - T_{i,j,1}^4)\Delta x_i \Delta y_j \tag{59}$$

where

T_a is the temperature of the surrounding surfaces,
σ is the Stefan-Boltzmann constant, and
ϵ is the emissivity of the fabric (assuming that α, the absorptivity, $= \varepsilon$).

The temperatures in equation (59) must be absolute (Kelvin) temperatures. In TMPSUB2 the temperature of the surrounding surfaces is assumed equal to the air temperature. (Note that equation (59) can be rewritten in an apparently linear form similar to equation (58):

$$(S_r)_{i,j,1} = [\sigma\epsilon(T_a + T_{i,j,1})(T_a^2 + T_{i,j,1}^2)](T_a - T_{i,j,1})\Delta x_i \Delta y_j \tag{59a}$$

This form will be useful further on.

The heat flux from a smoldering cigarette to the fabric is, for the "prescribed flux" choice of input, represented by the following pair of equations:

$$\phi_s(x,y,t) = \phi_{max}\exp\left[-\left(\frac{x - x_o - vt}{\sigma_{x+}}\right)^2 - \frac{y^2}{\sigma_y^2}\right] \qquad (x \geq x_o + vt) \tag{60a}$$

and

$$\phi_s(x,y,t) = \phi_{max}\exp\left[-\left(\frac{x-x_o-vt}{\sigma_{x-}}\right)^2 - \frac{y^2}{\sigma_y^2}\right] \qquad (x<x_o+vt) \tag{60b}$$

This heat flux is converted to a heat gain, S_s, by multiplying the flux at the position of the node by the cell surface area. These values are adjusted slightly so that their (discrete) sum is equal to the total heat flux represented by equations (60a,b):

$$\int_{-\infty}^{\infty}\int_{-\infty}^{\infty}\phi_s\,dx\,dy = \frac{\pi}{2}\phi_m\sigma_y[\sigma_{x+}+\sigma_{x-}] \tag{60c}$$

3. Air Gap

Since the furniture (apart from the frame) consists of fabric-covered padding, it is clear that the program must take at least two layers (with different properties) into account. Therefore the program was written so as to permit different values for the relevant thermophysical constants ρ, c, and κ at each node. In fact, generally there is not perfectly intimate thermal contact between the fabric covering and the padding: there is a small but sometimes significant intervening air gap. Normally, one would place a node within this gap, in order to take a third layer into account; because of the thinness of the gap, and other technical difficulties, however, a different treatment of the effect of this air gap has been devised: the gap can be represented in terms of its "thermal resistance."

The optional air gap between the fabric and the padding is modeled by assuming one-dimensional heat transfer. Figure 2 shows the basic configuration and nomenclature for an air gap of thickness s between cells i,j,k and i,j,k+1. s is small relative to the separation between the cells, δ_{k+1}. Although pyrolysis of the fabric and the possible melting and/or pyrolysis of the padding may well change the dimensions of the air gap, the simplifying assumption is nevertheless made here that the air gap has fixed and uniform dimensions. The heat transfer between these cells is given by

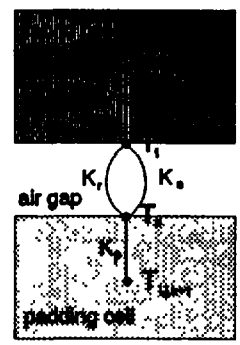

Figure 2. Air gap heat transfer model

$$q_{i,j,k+} = K(T_{i,j,k}-T_{i,j,k+1}) \tag{61}$$

where K is an implicit function of $q_{i,j,k+}$, $T_{i,j,k}$, and $T_{i,j,k+}$.

The overall heat transfer coefficient is given by

$$K = \frac{1}{\frac{1}{K_f} + \frac{1}{K_p} + \frac{1}{K_r + K_c}}$$

where the fabric conductance is

$$K_f = 2\Delta x_i \Delta y_j \kappa_{i,j,k} / \delta_{k+1} \ ,$$

the padding conductance is $K_p = 2\Delta x_i \Delta y_j \kappa_{i,j,k+1} / \delta_{k+1}$,

the fabric (bottom) surface temperature is $T_f = T_{i,j,k} - q_{i,j,k+} / \kappa_{i,j,k}$,

the padding surface temperature is $T_p = T_{i,j,k+1} + q_{i,j,k+} / \kappa_{i,j,k+1}$,

the radiant conductance is

$$K_r = \frac{\sigma \Delta x_i \Delta y_j (T_f + T_p)(T_f^2 + T_p^2)}{\frac{1}{\epsilon_f} + \frac{1}{\epsilon_g} - 1} \ ,$$

and the convective conductance is

$$K_c = \Delta x_i \Delta y_j \kappa_{air} / s \ .$$

The conductance of the air, κ_{air}, is evaluated at the average of T_f and T_p. These equations are solved to give K and $q_{i,j,k+}$ during the overall process used to compute cell temperatures.

4. Variable Grid

The heat from the cigarette spreads into the substrate by conduction. In order to correctly estimate the temperatures near the peak, it is important that conduction to the outer boundaries (at $x=0$, $x=x_{max}$, $y=y_{max}$, and $z=z_{max}$) be negligible, since it cannot be known *a priori*. This requires a relatively large region relative to the size of the cigarette heat flux pattern. However, setting Δx, Δy, and Δz sufficiently small to achieve the desired accuracy in the conduction calculation can result in an extremely large number of cells ($N = (x_{max}/\Delta x) \cdot (y_{max}/\Delta y) \cdot (z_{max}/\Delta z)$) with correspondingly large memory requirements and computation time.

The heating flux from a smoldering cigarette rises from negligible values to a high peak, on the order of 60 kW/m^2 over a region only a few millimeters in extent. In order to follow this faithfully, the region must be covered by a mesh which is fine enough so that there are no changes from one mesh point to another large enough to produce numerical inaccuracies or instabilities. Thus, the required size of the grid is inversely proportional to the temperature gradient, where steep temperature gradients occur only near the point of peak heat flux. Therefore, a variable grid is used. This grid consists of a few constant-width cells near the peak followed by cells of regularly increasing size to the outer boundaries. The increase in cell size is based on geometric progression, and can be different for each axis. Thus, for example, $\Delta y_{j+1} = R_y \Delta y_j$ ($R_y \geq 1$). The general effect of this variable grid is shown in Figure 3. This is easy to implement in equation (45) which explicitly incorporates the grid sizes. The variable grid gives

results which are less accurate than a constant grid. A benchmark test indicates that the results for R = 1.23 differ by < 0.11% at t = 100 s. from those obtained for the constant grid case, with still smaller errors for R closer to unity. (See Table A-1, Appendix A.)

Note: In choosing a grid, the user determines four items, in each coordinate direction: the width of the constant-width cells in the fine-grid region, the number of such cells, the total number of nodes along that axis, and the total width in that direction. The program then does the arithmetic, and finds the corresponding value of R_i. If that is < 1, an error message will be returned. Likewise, if too many grid points result from the attempted selection, an error message will result.

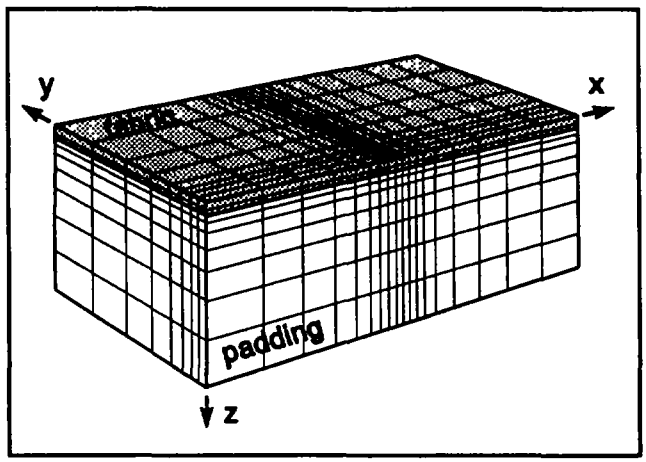

Figure 3. Substrate coordinate system

The point of peak heat flux moves as the cigarette smolders. TMPSUB2 adjusts the x-coordinates to keep the fine grid region centered on that peak. This adjustment is made by

(1) computing the new x-coordinates of the shifted grid,
(2) computing a cubic spline curve for the temperature in each row of cells in the old grid, and
(3) using the curve to compute the cell temperatures in each row at the new grid positions.

The standard explicit algorithm for solving equation (12), without pyrolysis included, was checked in several ways, principally by comparing its predictions against known analytical solutions. (See Appendix A.) These checks showed that the numerical procedure, and the computer program for implementing it, are correct, effective, and accurate.

5. Variable Thermal Properties

The conductivity and specific heat of the substrate materials are known to vary with temperature. TMPSUB2 allows the user to describe this variation. The values entered for κ and c are converted to cubic spline curves giving $\kappa(T)$ and c(T). The conductivity is further adjusted within the program to take into account the fact that the thermal conductivity is proportional to the density:

$$\kappa = \rho \, \kappa(T) / \rho_0, \tag{62}$$

where ρ_0 is the original density (recall that the assumption of constant κ, ρ, and c, in Section II.B.3, was a special case used only in order to obtain equations (17) to (19)).

6. Pyrolysis

Consider pyrolysis from the finite difference viewpoint. We begin with a cell having constant volume, ΔV (= $\Delta x \, \Delta y \, \Delta z$) and temporarily ignore the subscripts i,j,k. This cell contains a mass $\rho_v \, \Delta V$ of virgin (unpyrolyzed) material, a mass $\rho_c \, \Delta V$ of char, and a mass $\rho_a \, \Delta V$ of ash. The numerical method must

keep track of the density of each material as a function of time; in this program, this is done *via* the difference equation

$$\rho_{x,n+1} = \rho_{x,n} + \Delta t\, \dot{\rho}_{x,n+\beta} \tag{63}$$

where the subscript x may be v, c, or a, and β indicates the type of time integration, as discussed above. $\dot{\rho}_x$ is modeled using equations (25a,b,c). Note that $\rho_a = \rho_c = 0$ and $\rho_s = \rho_v = \rho_o$ at t = 0.

Some material is converted to gases during pyrolysis; the rate as which gases are created is given by equation (25e). The gases are lost from the cell, and they carry away all the energy they contain, *i.e.*, there is an enthalpy loss which does not affect the temperature of the remaining mass. Moreover, since the gas diffusion equations have not been explicitly included, any possible loss of heat from the escaping hot gases to the cooler solid in other regions of the substrate is ignored. Thus, the rate of heat gain in the cell due to pyrolysis is (almost exactly) given by

$$S_p = \Delta V(R_d H_d + R_{op} H_{op} + R_{co} H_{co} + \dot{\rho}_s c T) \qquad \text{Watts} \tag{64}$$

The R_i are given in Section II.B.3, and $d\rho_s/dt$ is given by equation (25e).

7. Time Integration

A choice must be made for the time integration method. Following the discussion of Belytschko (1983, pp. 55, 419, 445), the advantages of explicit time integration are:

(1) fewer calculations per time step;
(2) simple algorithm logic and structure are simple, implying that it is good for testing new ideas;
(3) ease of handling complex nonlinearities;
(4) requirement of little core storage compared to implicit methods using direct elimination procedures; and
(5) high reliability in terms of accuracy and completing the computation.

The only notable disadvantage is that explicit time integration is only conditionally stable so that a very large number of time steps may be required.

With regard to accuracy, since implicit methods are unconditionally stable, they can easily be used with too large a time step, leading to significant time integration errors. The stability requirements for explicit time integration force the time step to be so small that the time integration error is almost always smaller than the spatial discretization error. Of course, it is also possible to use a spatial discretization that is much too large.

The addition of pyrolysis to the model required significantly smaller cells in the region of interest, and therefore required significantly longer execution time. Hence a better method than explicit time integration was required. The following method attributed to Saul'yev as described by Larkin (1964) and Clausing (1969) was adopted:

Again consider the one-dimensional presentation of Figure 1. Assume that the calculation of cell temperatures is proceeding in the positive x direction. Then at cell i, $T_{i-1,n+1}$ is a known quantity and can be used in computing $T_{i,n+1}$. Equation (51) becomes

$$\Delta U_{i,n\to n+1} = C_{i,n+1}T_{i,n+1} - C_{i,n}T_{i,n} = \Delta t(q_{i-,n+1} + q_{i+,n} + S_{i,n+\beta}) \tag{65a}$$

During the next time step, calculate cell temperatures in the negative x direction. In that case equation (51) becomes

$$\Delta U_{i,n\to n+1} = C_{i,n+1}T_{i,n+1} - C_{i,n}T_{i,n} = \Delta t(q_{i-,n} + q_{i+,n+1} + S_{i,n+\beta}) \tag{65b}$$

Both equations (65a) and (65b) are unconditionally stable because of the inclusion of the implicit terms; operating together, the truncation errors during successive time steps tend to cancel leading to an $O(\Delta t^2)$ algorithm. This method is directly expanded into 2 or 3 dimensions by adding the j and k position indices and the q_{j-}, q_{j+}, q_{k-}, and q_{k+} heat gains. The key factor is that it is only necessary to solve implicitly for one cell temperature at a time. There are no time-consuming simultaneous equations to be solved. Tests indicate that this method is very accurate except for the possibility of some small oscillations as with the Crank-Nicholson method.

A question remains on when to evaluate S_i, C_i, and κ_i (which is implicit in the q's) in equation (65a). Numerical errors are minimized by evaluating S_i at time step $n+\frac{1}{2}$. These terms are all functions of temperature in the SUBSTRAT program. Furthermore, they are such complicated functions that the equations cannot be solved directly. The following equation must be solved implicitly for $T_{i,j,k,n+1}$:

$$\begin{aligned} U_{i,j,k,n+1} = U_{i,j,k,n} + \Delta t\,(& q_{i-,j,k,n+1} + q_{i+,j,k,n} + q_{i,j-,k,n+1} + q_{i,j+,k,n} \\ & + q_{i,j,k-,n+1} + q_{i,j,k+,n} + S_{i,j,k,n+\beta}\,) \end{aligned} \tag{66}$$

where

$$U_{i,j,k,m} = \rho_{i,j,k,m}\,\Delta V_{i,j,k}\,c_{i,j,k,m}\,T_{i,j,k,m}$$

with m = n and n+1. The total solid density in the cell is the sum of the virgin, char, and ash densities [equation (25d)] and is a function of time due to the pyrolysis reactions:

$$\rho_{i,j,k,n+\beta} = (\rho_v + \rho_c + \rho_a)_{i,j,k,n} + \beta\,\Delta t\,(\dot{\rho}_v + \dot{\rho}_c + \dot{\rho}_a)_{i,j,k,n+\beta} \tag{67}$$

The cell pyrolysis for the time step is evaluated at $T = (T_n + T_{n+1}) / 2$, and component densities also at $\beta = \frac{1}{2}$. Equation (66) was rewritten in a form allowing numerical solution by a standard secant method (Conte, 1972, pp. 299-306). This completes the outline of Larkin's method. The net result of using Larkin's method is that the time step is no longer limited by grid size, and pyrolysis is modeled with a reasonable execution time.

D. EXPERIMENTS

1. Experimental Arrangement

The next step is to compare the results predicted by SUBSTRAT with experimental results, in which an electrical heater was substituted for a cigarette. The schematic of an experiment designed to measure time to ignition is shown in Figure 4. This consists of the heater element from an automobile cigarette lighter, fitted with a concentric jacket to permit an air purge. The purpose of the air purge is to keep evolved products from the sample from being ignited to flaming, rather than to merely smolder. The heating element is raised to varying temperatures, all of them high enough for the element to be glowing (500 - 900 °C). The purging jet comes through the jacket, past the face of the element, and then out normal to it, toward the sample. It picks up a good deal of heat as it travels through the device. The resulting flux distribution beneath the heating element is shown in Figure 5. As we would expect, it is axially symmetric; it is well fitted by a Gaussian profile. Note that the higher the temperature the disk is heated to, the higher is the peak flux.

The measured flux to the gauge is not the same as what the substrate sees, however, because the latter heats up, whereas the flux gauge does not; call the former ϕ_g and the latter, ϕ_s. It follows from equation (3) that

$$\phi_g = \phi_{rad} + \phi_c = \phi_{rad} + h(T_g - T_c) \tag{68}$$

where T_g is the temperature of the hot purging gas, T_c that of the (cold) gauge, and $\phi_s = \phi_{in}$. For the case where the substrate is being heated, however, the convective contribution goes down:

$$\phi_s = \phi_{rad} + h[T_g - T_s(t)] \tag{69}$$

where $T_s(t)$ is the temperature of the substrate, which increases continuously. Thus the total flux decreases monotonically. Although we do not know the gas temperature T_g, we do not need it; for, we can combine equations (68) and (69) to obtain

$$\phi_s(t) = \phi_g - h[T_s(t) - T_c] \tag{70}$$

The heat transfer coefficient h was discussed in Section II.B. It is found for this experimental configuration in Appendix D. Analysis of the experimental results, given in Appendix D, yields a number of values important for this experiment, including h and the disk temperatures; the results are shown in Table D-1; h is found to be a weak function of ϕ_{ext}.

When a mock-up consisting of flexible PU foam covered by #12 cotton duck was placed in position under the heat source, smoldering ignition occurred after a certain amount of time; the ignition delay depends on the intensity of the flux, as indicated qualitatively by equation (19), Section II.B.2. The experimentally obtained ignition delays are plotted in Figure 6 as a function of the peak heat flux.

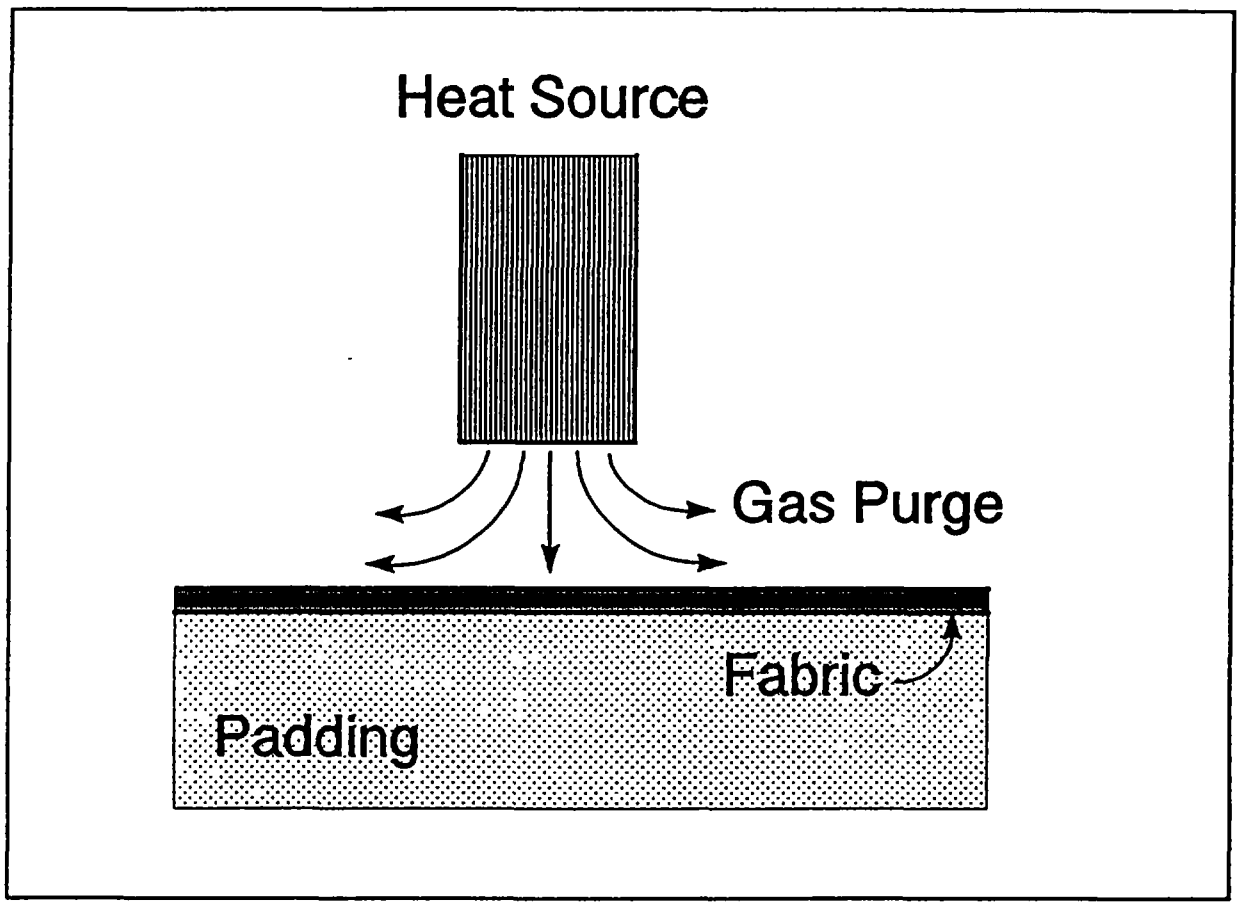

Figure 4. Schematic of heat source for ignition tests

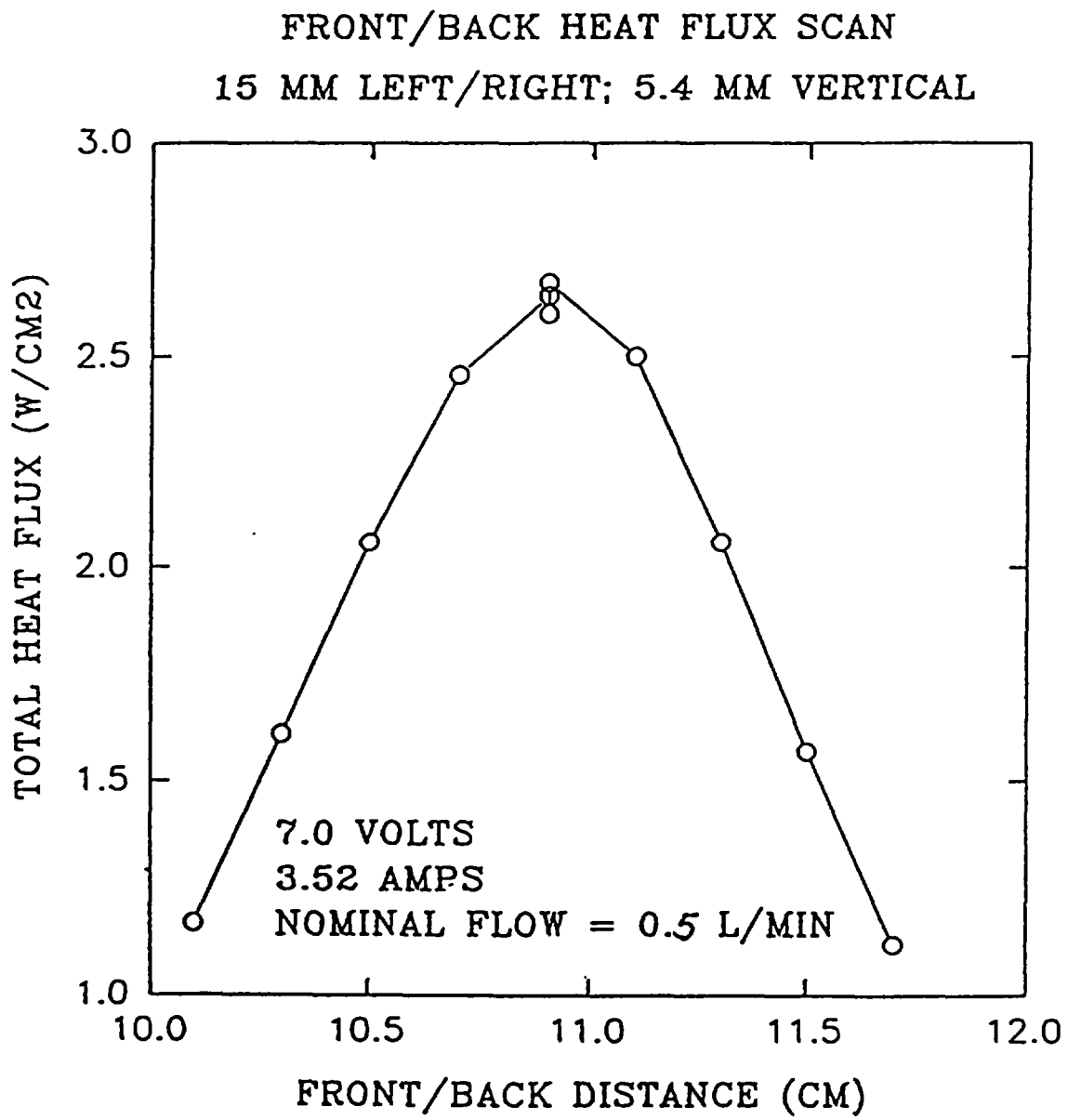

Figure 5. Flux profile from heat source, as measured by a total heat flux gauge

The ignition delay times as a function of the external flux are given in Table 2.

Table 2. Substrate Ignition Delay Times

ϕ_{ext}(kW/m^2)	18	25	34.5	44
t_{ig}(s)	472	70	37	22

Since ϕ_{net} is constant for each run, then according to equation (19), a plot of ϕ_{ext} versus $t_{ig}^{-1/2}$ should yield a straight line whose intercept is the critical flux, ϕ_{crit}. When this is done, however, the result is not a straight line. More generally, then, we assume that the relationship has the form

$$\Delta\phi \equiv \phi_{ext} - \phi_{crit} = A\, t_{ig}^{-p} \tag{71}$$

Only the correct choice for ϕ_{crit} will yield a straight line in a logarithmic plot of $\Delta\phi$ *vs* t_{ig}. When that is obtained, the slope of the line is -p; it was found that $\phi_{crit} \cong 16.9$ kW/m^2 and that $p \cong 1.087$, with A varying from 757 to 816; the average value is 798. If we take $p = 1$, A increases slowly with ϕ_{ext}.

The fact that $p \approx 1$, rather than 1/2, indicates that the substrate behaves like a **thermally thin** material; that, in turn, suggests that it is principally the fabric which is involved in the heating and ignition. If we assume that the principal cooling mechanism is radiation, then $\phi_{crit} \cong 16.9$ kW/m^2 implies that if the radiative absorption coefficient of the fabric is $\alpha = 0.9$, then $T_{ig} = 759$ K ≈ 485 °C -- a remarkably high value. Even with $\alpha = 1.0$, $T_{ig} = 739$ K = 466 °C, considerably greater than the 400 °C measured independently. This shows that there is substantial convective cooling during the heating/ignition process.

2. Material Data

In order to see whether the program can calculate t_{ig} correctly, it is necessary to calculate the surface temperature under the heater. In order to do that, however, it is necessary to have correct input data. Among these data are the thermophysical data, $\kappa\rho c$.

Fabric. First, consider the fabric. The fabric that was used in the experiment was #12 cotton duck. Material data for cotton, especially as a function of temperature, are surprisingly difficult to find, even though it is a common and long-used material.

In Appendix E, we find that reasonable values for the thermophysical constants for this particular cotton fabric (#12 cotton duck) are

$$\rho = 620\ kg/m^3$$

and

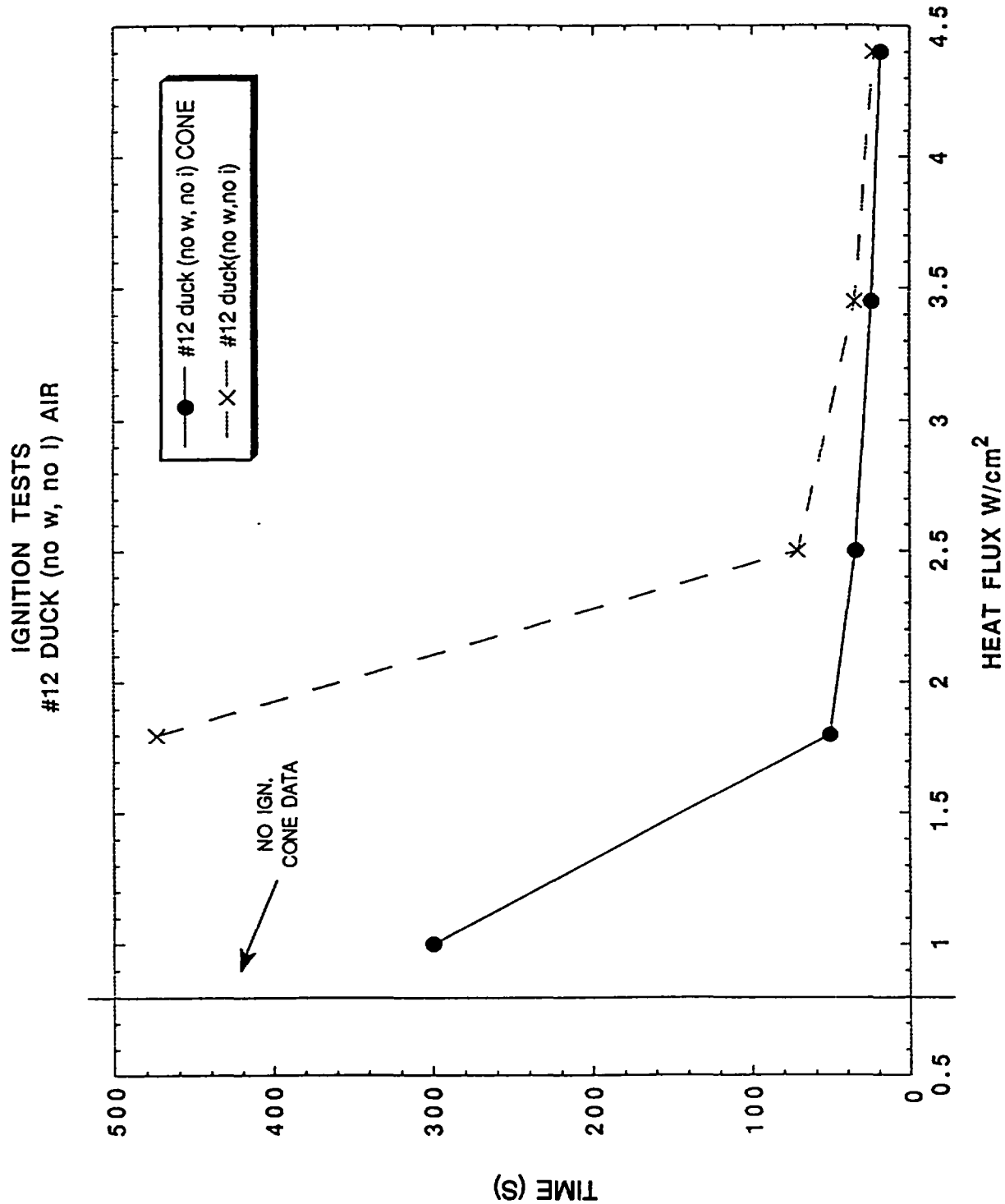

Figure 6. Time required to ignite the fabric, for different (initial) heat flux exposures. Crosses correspond to the discussion in the text. Filled circles correspond to a different set of experiments.

$$\kappa(T) = 0.28505\,\kappa_s(T) + 0.84554\,\kappa_{gas}(T) \qquad W/m\text{-}K \tag{72}$$

where

$$\kappa_s(T) = \kappa_s(T_a)\,(T/T_a) = 1.242\times10^{-3}\,T \quad W/m\text{-}K \tag{73}$$

(with T in Kelvins) and $\kappa_{gas} = 1.7\,\kappa_{air}$, with

$$\kappa_{air} = \frac{a\sqrt{T}}{1 + \dfrac{b\times10^{-cT}}{T}}\ , \tag{74}$$

The constants are: a = 2.6464x10^{-3}, b = 245.4, and c = 12. Then κ(25 °C) = 0.1435 W/m-K and c(T) = κ(T)/$\rho\alpha$ $\approx$ 7819κ(T); thus, c $\approx$ 1122 J/kg K at 300 K.

Char. The cotton decomposes and pyrolyses to form char. According to Parker (1985, 1988), the specific heat of char is just about that of carbon:

$$c_c(T) = 1.43 + 3.55\text{x}10^{-4}\text{T} - 7.32\text{x}10^{4}/\text{T}^2 \qquad \text{J/g-K, with T in K} \tag{75}$$

The thermal diffusivity of wood char is approximately constant:

$$\alpha_c \approx 2.1\text{x}10^{-7}\ \text{m}^2/\text{s} \tag{76}$$

The density of the char depends on whether the fibers contract while pyrolyzing, or not. Finally, the thermal conductivity of char is found from

$$\kappa_c(\text{T}) = \alpha_c\rho_c c_c(\text{T}). \tag{77}$$

Reaction Kinetic Parameters. When the analysis of a pyrolyzing material is carried out, it is done for a thin layer, in order to ensure uniformity of temperature and of oxygen concentration throughout the sample. It is then simplest to find the reaction rate in the form

$$k_d = \frac{d(W_d/W_o)}{dt} = A_d\left(\frac{W_d}{W_o}\right)^{n_d}\exp(-E_d/RT) \quad \text{min}^{-1} \tag{78}$$

for the degradation reaction, rather than as in equation (20); here $W_d = W_d(t)$ is the (instantaneous) weight of the remaining (virgin) material = weight of sample minus weight of char and ash, and W_o is the original weight. Note that A_d is commonly given in reactions/minute. The actual reaction rate is given by

$$R_d = \rho_o k_d.$$

The relationship between (20) and (78) is simple: since $\rho_d = W_d/V_d$ and $\rho_o = W_o/V_o$, then as long as V_o/V_d = const, $W_d/W_o = \rho_d/\rho_o$, and, as in equations (20),

$$R_d = A_d'\,\rho_d^n\exp(-...)$$

where

$$A_d' = A_d \rho_o^{1-n}$$

(in the appropriate units). For pyrolysis in pure nitrogen, Ohlemiller (1991) found:

$$A_d = 7.49 \times 10^{14} \text{ min}^{-1}, \quad n = 0.60, \quad \text{and} \quad E_A = 182.4 \text{ kJ/mol}$$

Instead of these parameters, however, we shall use the results of Kashiwagi and Nambu (1992) for a cellulosic paper pyrolyzed in air; that will maintain internal consistency in the reaction set. The global kinetic constants given by Kashiwagi and Nambu for the thermal degradation reaction of their cellulosic paper are

$E_d = 220$ kJ/mole $\qquad n_d = 1.8$
$A_d = 1.2 \times 10^{19}$ min^{-1} $\qquad H_d = -570$ J/g

The parameters for the other two reactions are given in their Tables 1 and 2, reproduced below. For the oxidative pyrolysis reaction,

$$k_{op} = A_{op} X_{ox}^{n_{ox}} \left(\frac{W_d}{W_o}\right)^{n_{fop}} \exp\left(-\frac{E_{op}}{RT}\right) \tag{79}$$

where X_{ox} is the volume fraction of oxygen. The kinetic constants are:

$E_{op} = 160$ kJ/mol $\qquad n_{op} = 0.5$
$A_{op} = 1.5 \times 10^{14}$ min^{-1} $\qquad n_{fop} = 1.3$

and: $\qquad H_{op} = 5.7$ kJ/g

For the char oxidation reaction,

$$k_c = A_c X_{ox}^{n_{co}} \left(\frac{W_c}{W_o}\right)^{n_c} \exp\left(-\frac{E_c}{RT}\right) \tag{80}$$

with the kinetic constants

$E_c = 160$ kJ/mol $\qquad n_{co} = 0.78$
$A_c = 3.4 \times 10^{11}$ min^{-1} $\qquad n_c = 1.0$

and $\qquad H_c = 25$ kJ/g

The fraction of ash which remains is 9% by mass. Equations (79) and (80) transform to the standard form in the same way that (78) does. Thus

$$A_{op}' = A_{op} \rho_o^{1-n_{fop}} \rho_a^{-n_{op}}$$

$$A_o' = A_c \rho_o^{1-n_c} \rho_a^{-n_{co}}$$

Heats of Combustion. Brandrup and Immergut (1989) give the heat of combustion from several measurements; as expected, the results vary:

H_c(cotton) ≈ 18850 J/g
H_c(fabric1) ≈ 15450 J/g
H_c(fabric2) ≈ 16700 ± 250 J/g (fabric weight was 180 g/m^2)

Note: as material pyrolyzes, we should take c(T) and κ(T) for the combination of materials; for the sake of simplicity, however, we assume that the virgin fuel, the pyrolyzed material, the char, and even the ash, all have the same specific heat. Then the appropriate density to use in equation (12), for example, is the density of the solid, ρ_s, which is the sum of the bulk densities of all the components of the solid (see equation (25d)). As pyrolysis and combustion proceed, ρ_s decreases monotonically, assuming no fabric shrinkage.

Foam. For the padding component of the substrate, we have PU foam, for which we have the following data (Ohlemiller, 1991):

$$\rho = 0.032 \text{ g/cm}^3 = 32 \text{ kg/m} \tag{81a}$$

$$c_p = 1.46 \text{ J/g K} \tag{81b}$$

and $$\kappa(T) = 0.03613 + 2.003\text{x}10^{-4}\, T, \tag{81c}$$

with T in °C.

There is one other datum for PU foam: $<\kappa\rho c>$, the mean value of the thermal inertia, was measured in the LIFT apparatus (Quintiere *et al.*, 1983, Quintiere and Harkleroad, 1985, Quintiere, 1988). However, the foam melts before it ignites, so that ρ (and, consequently, κ) go up substantially; moreover, the measurement entails all the other model approximations. Hence the measurement is not directly useful.

Foam Kinetic Parameters. The first pyrolysis reaction, which results in the collapse of the foam structure, yields 0.7 g of liquid and 0.3 g of vapor for every gram of foam which pyrolyzes. The reaction rate, RR_1 = (mass gasified/min)/(mass of foam), is given by

$$RR_1 = 0.30B\left(\frac{\rho - \rho_R}{\rho_o - \rho_R}\right)^m \exp\left(-\frac{E_B}{RT}\right) \tag{82}$$

where m = 1.5
B = 3.36x10^{17}, and
E_B = 187 kJ/mol.

Also, ρ_o = starting density,
ρ = current density, and
ρ_R = density of residue ≈ 0.70ρ_o.

These densities are those of the solid phase (ρ_o of order 1g/cm^3), rather than that of the foam (ρ_o ≈ 0.03 g/cm^3). The total heats of pyrolysis of PU foams range between 400 and 800 J/g; for this foam, it is closer to the upper value. Assuming it varies linearly with the mass loss, we can estimate 30% of 800, or

$$H_p \sim 240 \text{ J/g}$$

Finally, for the diffusion coefficient for O_2 in the fabric, see equation (28).

E. RESULTS AND DISCUSSION

Rather than give the final results immediately, it was decided to describe the evolution of our thinking, including some of the false steps we took, because a good deal can be learned that way, and it could be instructive for anyone else who might work on this problem in the future. With that in mind, we first consider the results of calculations made assuming an inert substrate.

1. Inert Substrate

First, the computer program was used to calculate the peak surface temperature under the heater as a function of time for several peak fluxes. The results are shown in Figure 7.

The ignition temperature of cotton was measured to be 390-400 °C (Ohlemiller, 1991). According to Figure 7, if $T_{ig} \approx 400$ °C, then ignition is attained for the 44 kW/m^2 exposure at $t \approx 18$ s, and for the 34.5 kW/m^2 exposure at $t \approx 50$ s. These values compare very favorably with experimental values of 22 and 37 s, respectively.

On the other hand, ignition is not attained at all for the 25 and 18 kW/m^2 cases, while the calculation predicts the substrate will reach the ignition temperature, albeit at long exposure times. A conceivable reason might be that the ignition temperature given above was overestimated. In order to intersect the $\phi = 18$ kW/m^2 curve at $t \approx 472$ s, the ignition temperature would have to have been about 290 °C; it is very unlikely that such a large error in the measurement of T_{ig} would have been made. Even if it were, that would yield ignition times of 7, 12, and 25 s, respectively, much shorter than the measured times of 22, 37, and 70 s.

[Three possible reasons why the calculated ignition times might be so short are:

(a) endothermic pyrolysis taking place, which slows the temperature rise;

(b) Significant radiative heat transfer within the material, so that the flux is absorbed in depth, rather than mainly at the surface; and/or

(c) $T_{ig} = 290$ °C and the estimates of $\kappa\rho c(T)$ were in error, the actual value being larger.

Now, if we consider endothermic pyrolysis, then we must also consider exothermic pyrolysis. Second, the effect of radiative heat transfer will be small when T is near T_a, and small in comparison with the effects of pyrolysis when $T >> T_a$. Finally, consider item (c): If $\kappa\rho c$ were larger, then the rate of rise of T_s would be smaller, as can readily be seen from equations (17)-(19). The final temperature, however, is independent of $\kappa\rho c$. Hence not only would T_{ig} have to be much smaller, but the estimates of $\kappa\rho c$ would have to have been 9 times too small. This is all possible, but extremely unlikely.]

2. Results with Pyrolysis

On the other hand, we know that pyrolysis must take place. Figure 8 shows the effect of including pyrolysis for the Q = 25 kW/m^2 case. Curve a indicates what the temperature of the fabric surface would be if the fabric (and foam) were inert. Curve b is the result of "turning on" the (endothermic) degradation reaction. Note that although the rate of growth of temperature is slowed down quite perceptibly, as expected, the temperature the surface reaches asymptotically is exactly the same (assuming the same surface absorptivity/emissivity as before).

However, the exothermicity of the oxidative pyrolysis and of char oxidation are far greater than the endothermicity of thermal decomposition, and should overwhelm it. We cannot, therefore, consider thermal decomposition alone: if we consider pyrolysis, we must include all the major reactions. Another way of seeing this is to note that in order to have ignition, we must have a "thermal runaway," where exothermic pyrolysis heats up the material faster than heat diffusion and surface losses can carry the heat away.

Curve c indicates what takes place when the oxidative pyrolysis reaction is included, as well: it is exothermic, and adds a great deal more energy than the degradation reaction removes. The result is, logically, that the temperature rises rapidly, almost like a thermal run-away. However, the temperature reaches a peak, than declines. The reason is simple: the fuel is rapidly exhausted. Once that happens, the heat source is reduced to the original external flux. This is clearly depicted in Figure 9, which shows the fuel density as a function of time. The ordinate is temperature, in °C, and density in kg/m^3. The curves marked T_0 and ρ_0 correspond to the cell with the highest temperature. Those marked T_1 and ρ_1 correspond to the (laterally) adjacent cells, and those marked T_2 and ρ_2 to the next ring of cells. These calculations were carried out assuming no char oxidation. We see that as the reaction accelerates, T_s "runs away" and the density plummets from its virgin value to that of char. Most significantly, the peak temperatures develop just after the density falls.

Finally, curved of Figure 8 shows the result of adding the char oxidation reaction as well: that additional heat source takes the pyrolysis "over the top." The temperature continues to run away. (We have arbitrarily cut off the calculation at 600 °C, here.) The question then arose: why was there an oscillation in T_s? The qualitative explanation is that if a cell is too large, then the surface/volume ratio is small, and the heat cannot diffuse away rapidly enough. This is confirmed by Figure 10. With a cell size taken to be a bit less than half as large, the amplitude of the oscillation declined considerably, and with the cell size halved again, the oscillations have almost disappeared.

Presumably, as we continue to decrease the cell size, the numerical errors should become progressively smaller, until a further decrease in cell size would make no further difference in the results. However, it was found that the results were apparently not converging with decreasing Δx, and that the sensitivity varied with Q. Investigation of the reason for this great sensitivity revealed that it lay in our use of a variable grid size: whereas for grids of constant spacing, the numerical approximations are correct to second order in Δx, that accuracy drops to somewhere between first and second order. Indeed, if the numerical error is proportional to $(\Delta x)^n$, then n is given by a complex formula (Torrance, 1985, pp. 43 and 51). The "flavor" of that expression is given by $n \sim (2+a)/(1+a)$, where $a \equiv \partial \Delta x/\partial x$. That is, the accuracy depends inversely on the rate of growth of the grid size. An explicit calculation is given in Appendix A; see Table A-1 there.

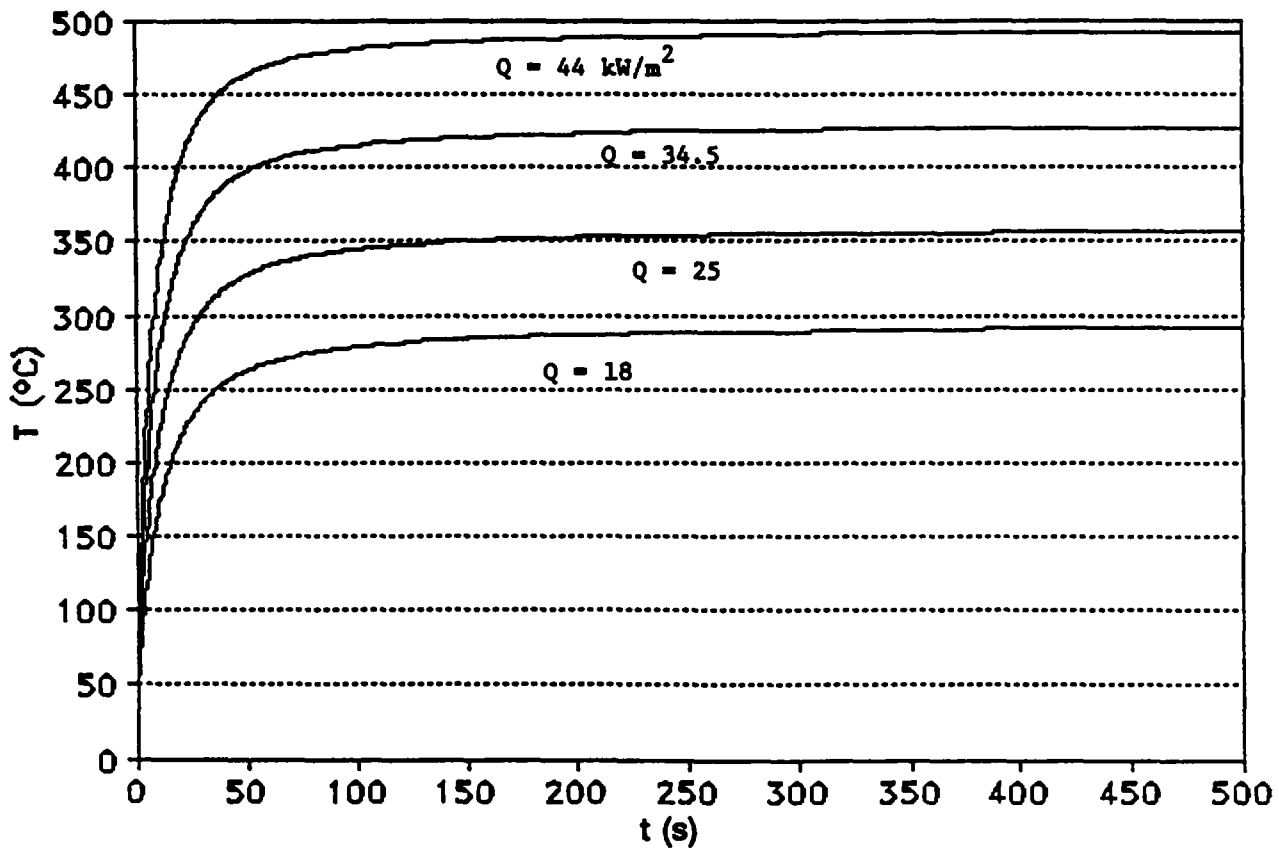

Figure 7. Peak surface temperatures of substrate as a function of time, for the four exposures

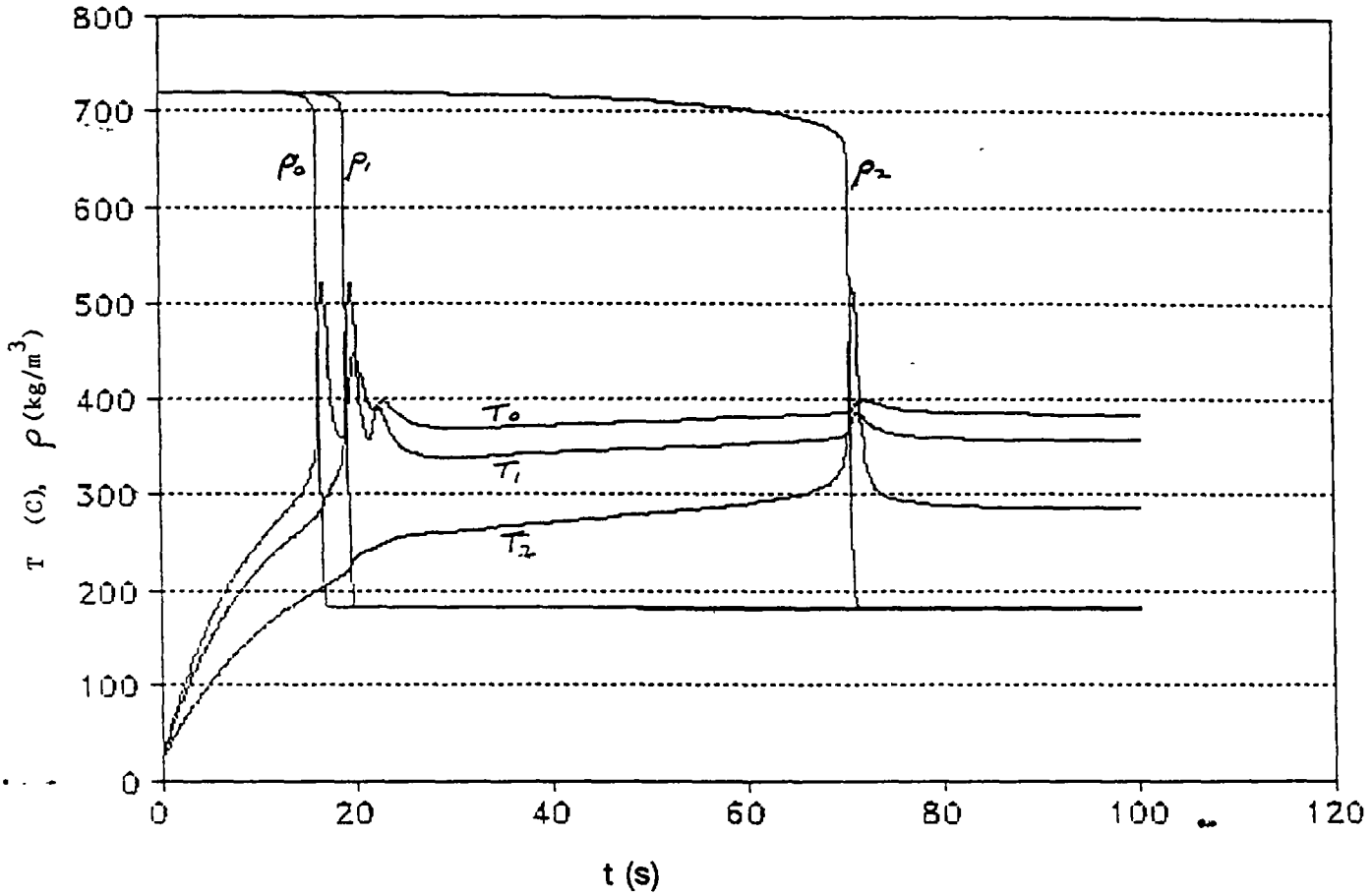

Figure 9. Temperature and density of central cell (subscript 0), adjacent cells (subscript 1), and cells in next ring around center (subscript 2), as functions of time

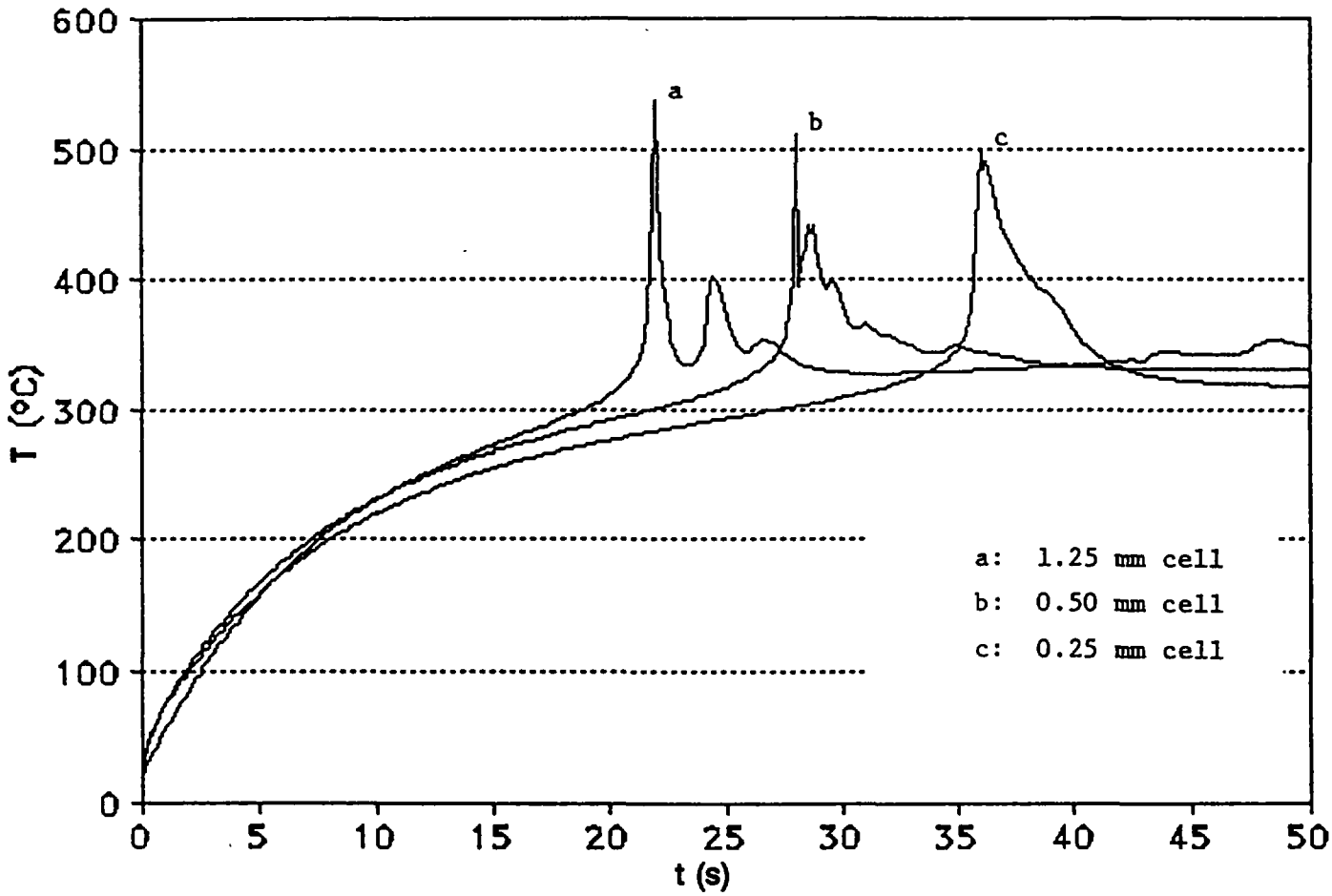

Figure 10. Temperature of central surface cell (i.e., peak temperature) for three different grid sizes: 1.25, 0.50, and 0.25 mm cubes. Char oxidation was purposely left out

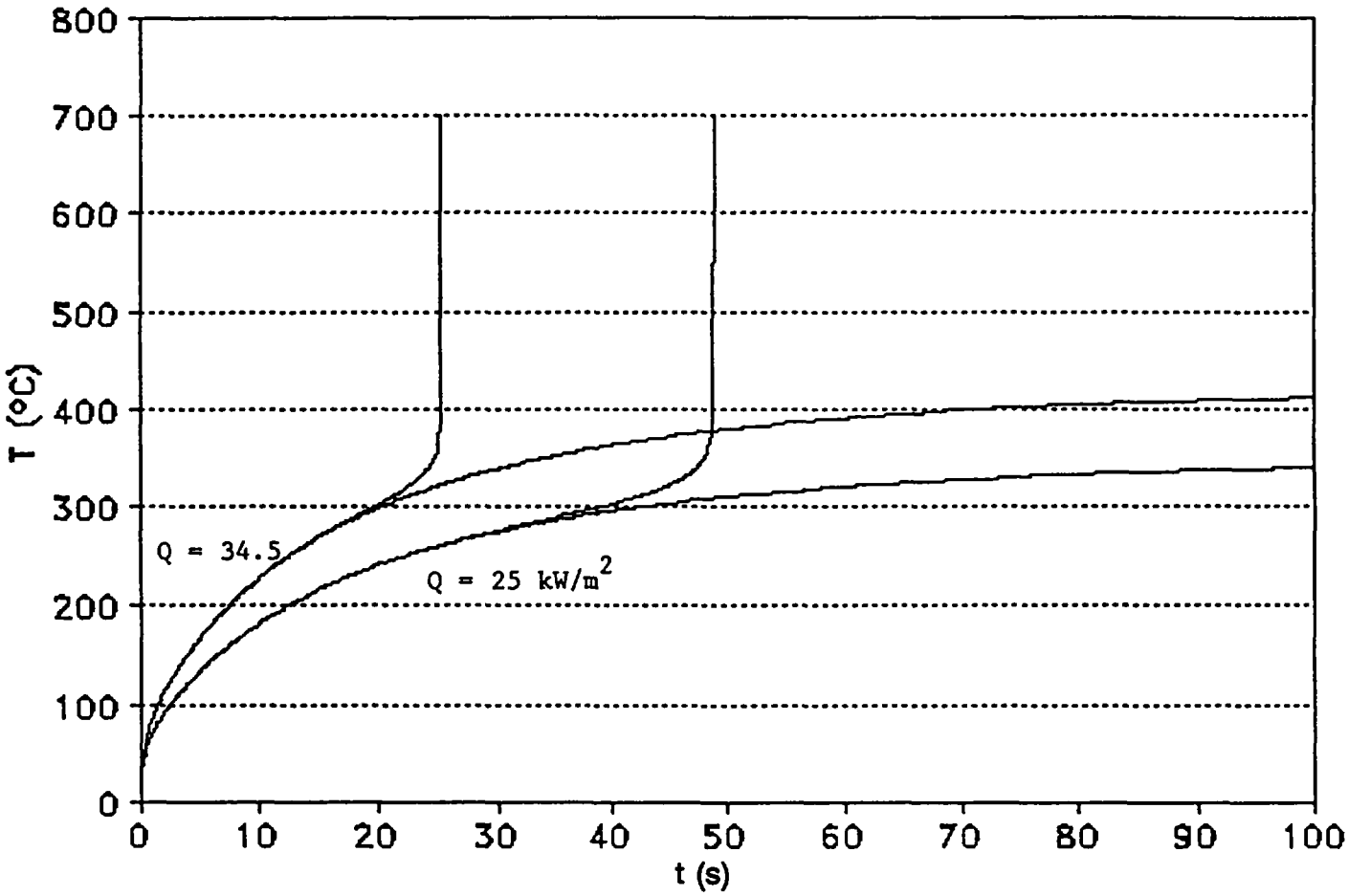

Figure 11. Peak temperature for the 25 and 34.5 kW/m^2 cases, assuming (a) no pyrolysis, and (b) all three pyrolytic reactions

By reducing the rate of increase of grid size, therefore, the accuracy was increased, and the results made to converge better. Moreover, it was decided to switch from an explicit solution method to Larkin's semi-implicit method (see Section II.C). After those changes, we arrived at the results shown. The results of four calculations are shown in Figure 11. These were made
with an assumed heat transfer coefficient h = 20, and an assumed oxygen concentration of 20%. For initial fluxes with peak values of 25 and 34.5 kW/m^2, calculations are first made assuming that the substrate is inert, and then pyrolysis is "turned on." We see that for the 34 kW case, the asymptotic temperature lies at about 430 °C, and that a thermal runaway begins at about 300 °C, at t $\approx$ 20, and is completed at t $\approx$ 25 s; that would then be the ignition time. It is difficult to state precisely what "the ignition temperature" is, in this case (but see below).

For the 25 kW case, the asymptotic temperature lies at about 360 °C. The first perceptible deviation of the curve for the reactive case from that for the inert material occurs at T $\approx$ 280 °C, and is clearly established at 300 °C. The thermal runaway takes place at t $\approx$ 48 s. These times may be compared with the experimentally-established ignition times, which were about 22 and 70 s, respectively. Thus we have achieved semi-quantitative agreement. In Figure 12, on the other hand, we see that a thermal runaway, and therefore ignition apparently did not take place for the 18 kW case. Here, the asymptotic temperature is about 290 °C; this is apparently not high enough to produce a runaway.

Wherein lies the difficulty? Most likely, one or more of the input values is incorrect. Altering $\kappa\rho c$ would principally change the time scale. Figure 13 shows the effect of changing the assumed oxygen concentration: the highest curve reproduces the upper curve in Figure 12. The next two curves show what happens when $<Y>$ is assumed to be 0.15 and 0.11, respectively. Finally, the bottom curve (again) corresponds to the inert case. Thus, it is not $[O_2]$ having been chosen too low that prevents ignition, and one or more of the kinetic parameters is probably in error. In Figure 14, curves a and b again reproduce Figure 12 (on a different scale). For curve c, the char oxidation rate was doubled. It is apparent that the curves overlap completely. A preliminary conclusion inferred from this was that the observed result was due to all the char that is produced already being oxidized. Observation of the kinetic constants for oxidative pyrolysis and char oxidation, however, makes it clear that the latter is three orders of magnitude slower than the former. Therefore merely doubling the char-oxidation rate will only perturb the energy output slightly -- so slightly that it will not even show up in the figure.

For curve d, the oxidative pyrolysis rate was doubled (the pre-exponential factor A was doubled), doubling the char-production rate through this branch; this indeed produced a thermal runaway. Curves e and f are the results of increasing A by 20% and 10%, respectively. Thus, a quite modest increase in A predicts ignition, although at 230 s, rather that the measured 472 s. Such an increment is not only well within experimental error, but is entirely plausible, when the likely differences between the cellulosic paper and a cotton fabric (with different impurities) are considered. On the other hand, it was assumed that y = 0.20. For y = 0.15, A must be increased by 30% in order to get ignition (the resulting T(t) curve is very similar to the "best" one). Although this is greater than the 10% increase found above, it is still entirely plausible.

We have so far considered the sensitivity of the results to the oxygen concentration, the thermophysical constants of the fabric, and its kinetic parameters. Surprisingly, there are two other significant parameters: first, if we use h = 22 for the heat transfer coefficient in equation (69) (as suggested by the results of Appendix D, shown in Table D-1), rather than the assumed h = 20, the "asymptotic" temperature (that at t = 500 s) reaches only 272 °C, rather than 292 °C, and there is not the faintest possibility of achieving ignition, unless E_A is substantially smaller than 160 kJ/g. One solution is to assume that h = 20 is the correct value to use, since the theoretical calculations in Appendix D could

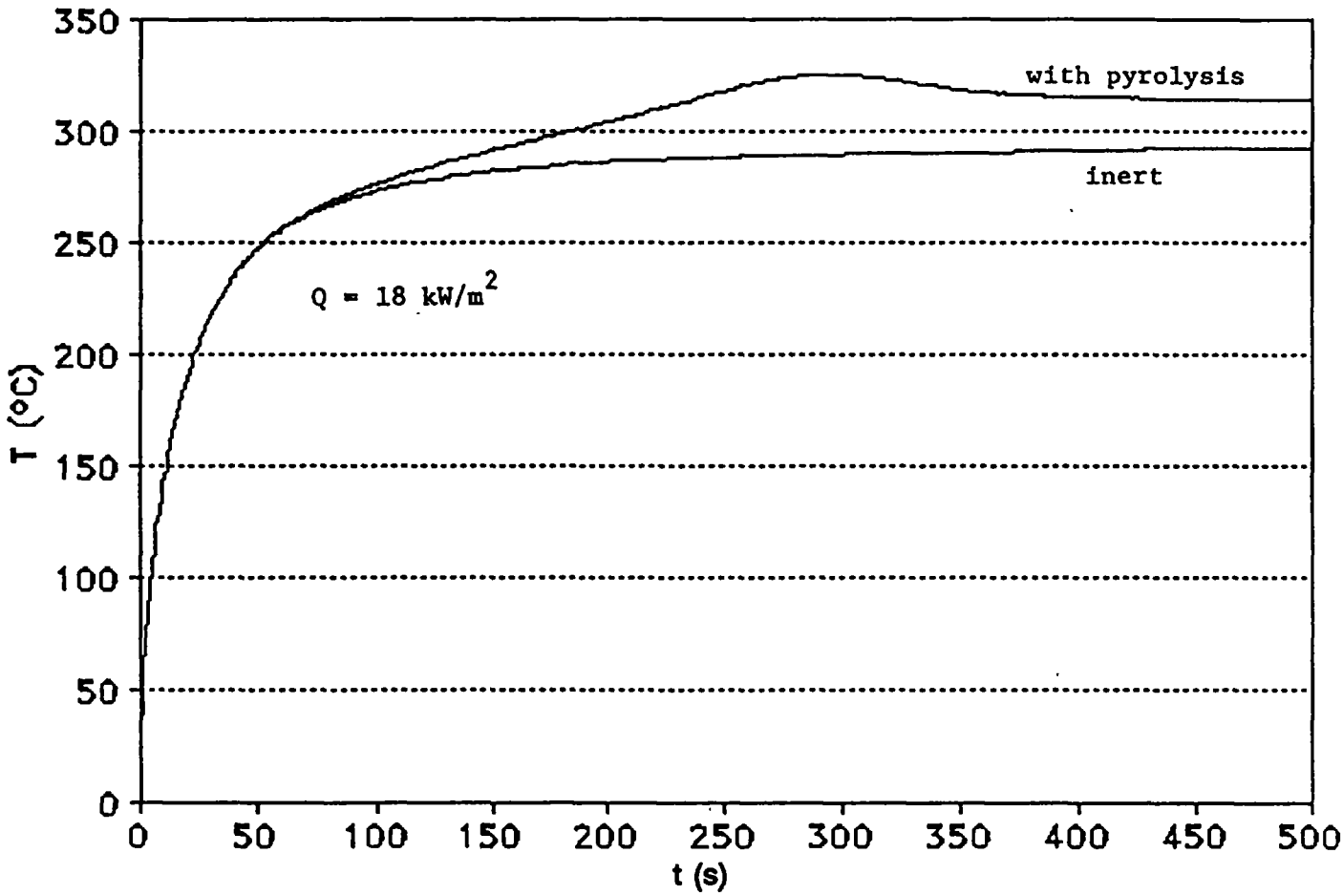

Figure 12. Peak temperature for the 18 kW/m^2 case, with the same assumptions as in Fig.11

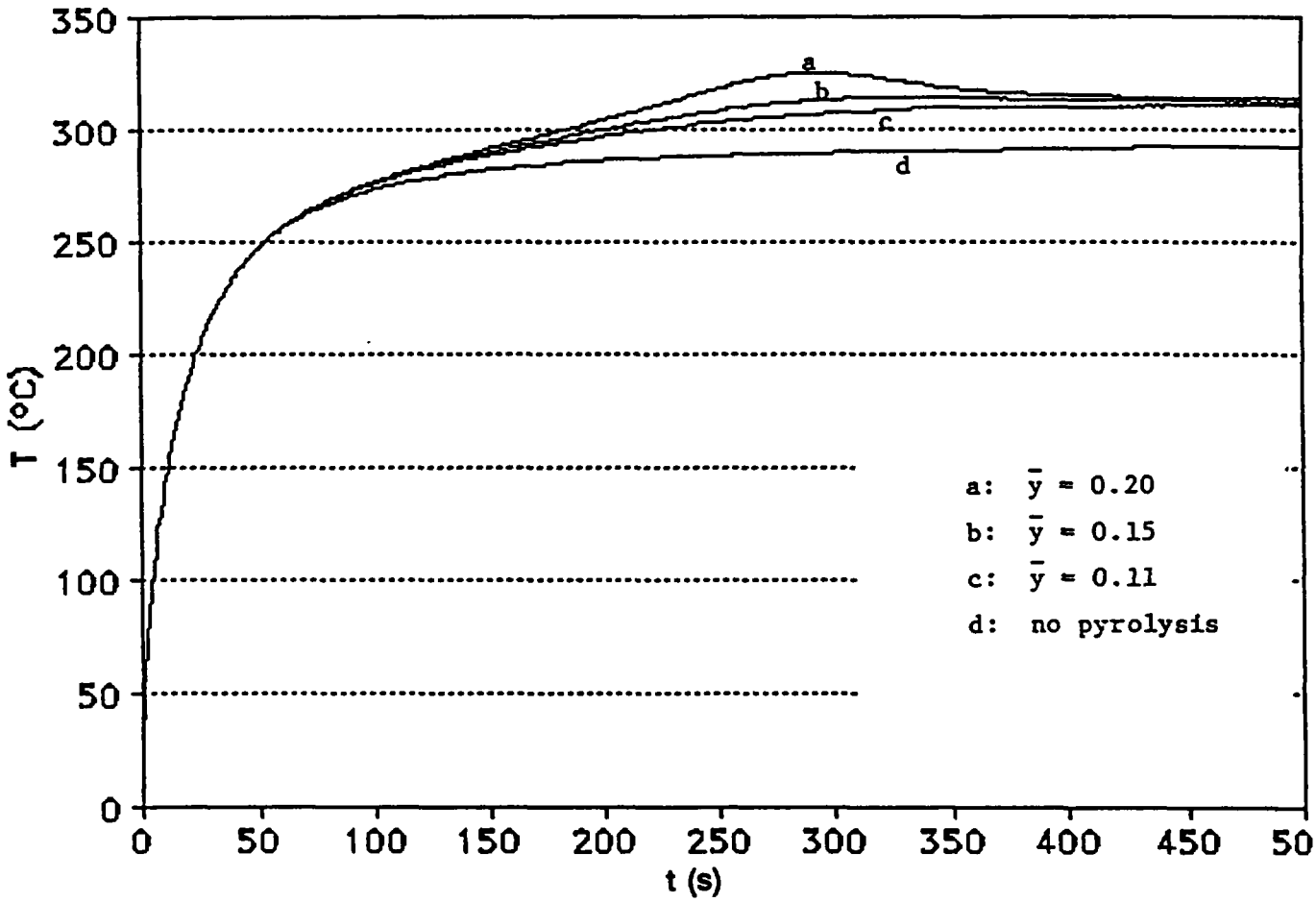

Figure 13. Peak temperature for the 18 kW/m^2 case, for several values of mean O_2 mass fraction, <y>

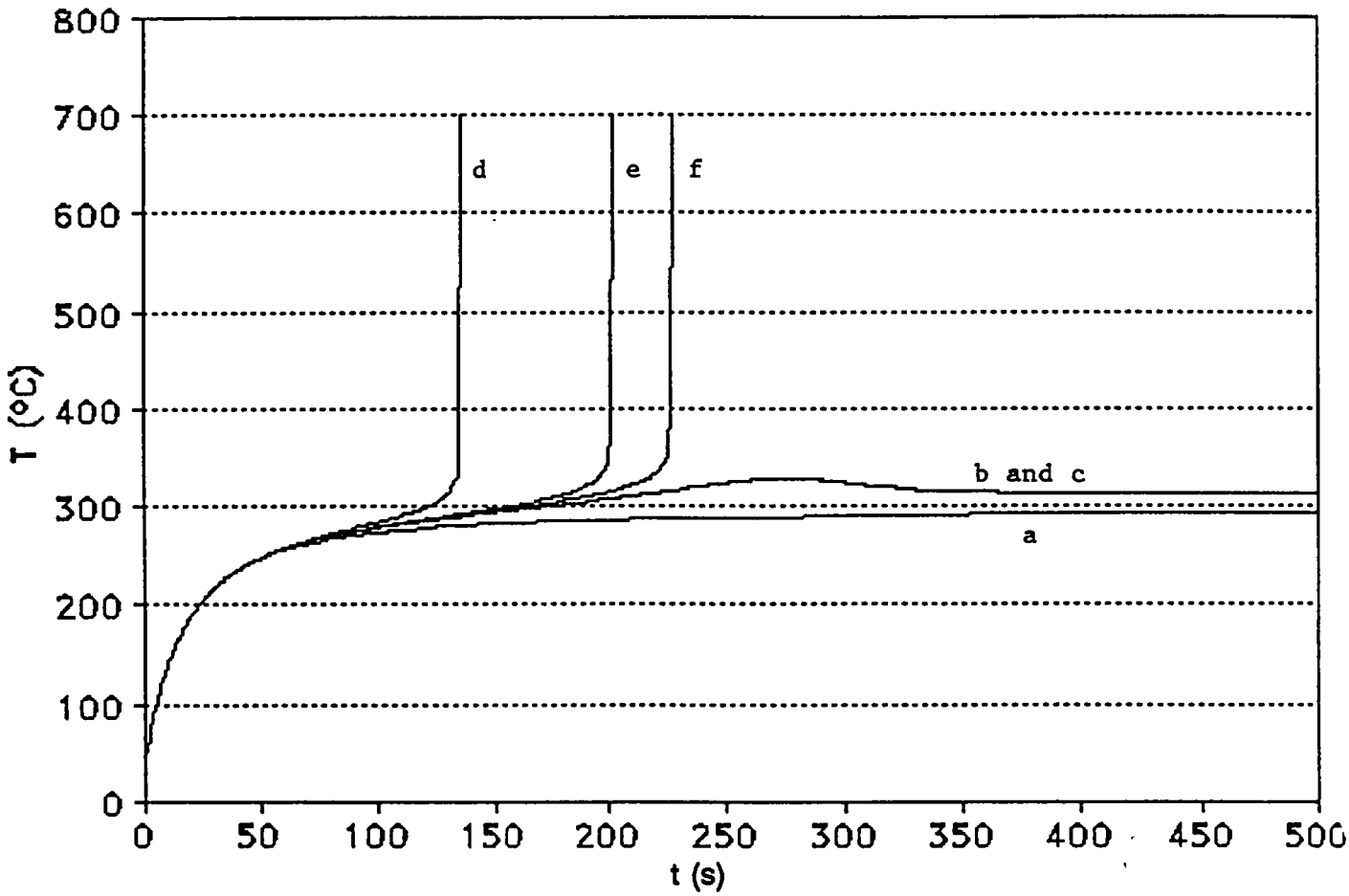

Figure 14. Peak temperature for the 18 kW/m^2 case, with various assumptions for the pyrolysis: Curve a, no pyrolysis; curve b, "standard" pyrolysis; curve c, double the char oxidation rate; Curve d, double the oxidative pyrolysis rate; Curve e, 1.2 times the oxidative pyrolysis rate; Curve f, 1.1 times the oxidative pyrolysis rate

easily be off by 10% or more. Another resolution is possible, too: the second parameter which is important in this threshold region ("threshold," because 18 kW/m^2 is close to the critical flux, 16.9 kW/m^2) is the thermal conductivity of the foam padding. In all the runs made above, it was assumed that κ = 0.056 J/m K and c = 1.9 J/g K, for the foam at T = 20 °C. If it were assumed that κ = 0.096, instead, then the foam would act as a more efficient heat sink, and the surface temperature could be expected to drop; indeed, a calculation showed that the peak surface temperature at t = 500 s fell to 272 °C for the inert fabric. In fact, however, the value 0.056 for the thermal conductivity was for a foam of density 48 kg/m^3! Transforming that for a 32 kg/m^3 foam, according to equation (62), yields 0.036, almost exactly what is given in the present test (see equation (81c)). This **reduces** the heat sink, and must yield an increased asymptotic surface temperature. Using the foam parameters given by equations (81), and h = 20, the t = 500 temperature indeed rises, from 292 °C to 300 °C; with h = 22, it is 294 °C, and we only need to increase A by 10% to get runaway.

The "best" set of parameters for the fabric and foam, then, is given in Section II.D.2. For the heat transfer coefficient, use the values in Table D-1. With that set, we obtain the curves shown in Figure 15. The corresponding calculated ignition times are given in Table 3. The calculated values are all about half the measured values, and the trend is well-predicted.

Note that the polyurethane foam begins to melt and recede from the fabric when its temperature reaches about 300 °C, thereby decreasing the heat-sink effect of the padding, and accelerating the heating of the fabric. This effect has not been included in the model.

Table 3. Comparison of Substrate Ignition Delay Times

	Ignition delay, t_{ig} (s)	
Q (kW/m^2)	Calculated	Measured
18	209	472
25	37	70
34	19	37
44	13	22

It has been suggested that we might avoid the necessity of explicitly including the pyrolysis reactions by choosing some effective ignition temperature. This is not, in fact, feasible: if we take the measured ignition times and mark them on the four curves in Figure 7, corresponding to the inert assumption, we find that they intersect these curves at widely varying temperatures; see Table 4. It is apparent that this "ignition temperature" is a strong function of the external flux.

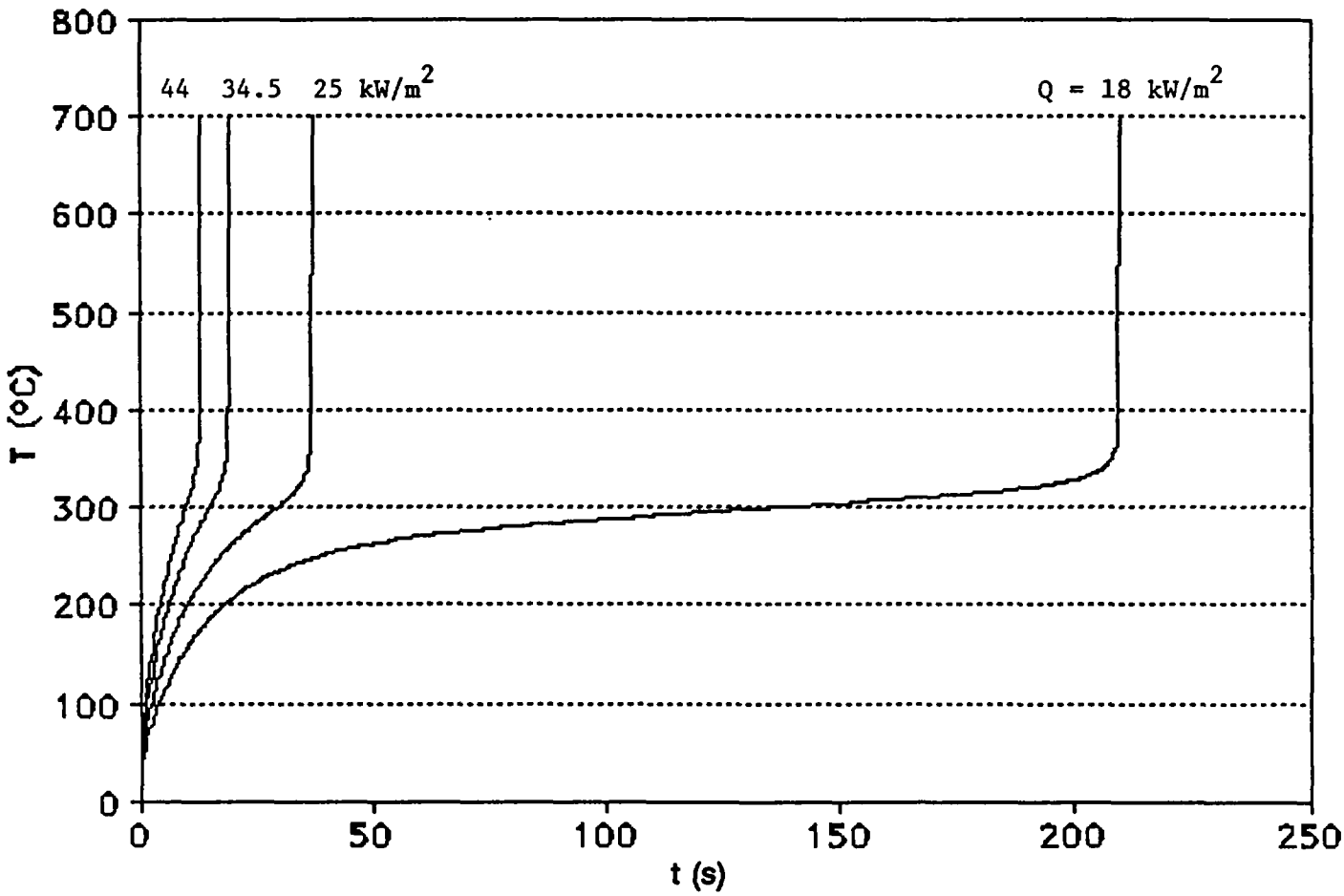

Figure 15. Peak temperature as a function of time, for all four cases, using the best set of input data

Table 4. Surface Temperatures Which Would be Attained by the Substrate at the Measured Ignition Times If the Substrate Were Inert

ϕ_{ext} (kW/m^2)	18	25	35	44
T_{ig} (°C)	291	342	380	400
T_{ig} (K)	564	615	653	673

On the other hand, if we define "the ignition temperature" as the point on the $T_s(t)$ curve where the temperature is rising at some rapid rate, *e.g.*, 100 °C/s, then from Figures 11 and 13 we see that that gradient is attained at the approximate temperatures shown here:

Table 5. Surface Temperatures at a 100°C/s Rate of Rise (Data From Figures 11 and 13)

ϕ_{ext} (kW/m^2)	18	25	35
T_{ig} (°C)	390	390	380
T_{ig} (K)	663	663	653

These calculated temperatures are close to each other, and close to the 390-400 °C which has been measured.

F. SUMMARY FOR SECTION II

We have created several computer programs, of which the central one is SUBSTRAT2. This program calculates the temperature history at every point in a substrate (the upholstered furniture) which is subjected to a strongly localized heating flux on its top surface (assumed to be horizontal). The (solid) substrate consists of two layers, the top one being a fabric and the lower a foam pad; there may be a thin intervening air gap. The substrate is taken to be a rectangular parallelepiped, and it is broken up into several thousand cells. The ambient oxygen level can be set at whatever value one wishes.

The solid is subjected to a nonuniform and time-varying heating flux at its top surface, and (simultaneously) experiences convective and radiative heat losses. Moreover, the solid can undergo pyrolitic reactions; we consider three, here: one endothermic step (thermal degradation to char), one oxidative pyrolysis to char, and oxidation of the char (to ash). The way T(r,t) is found is by solving the PDE which describes the diffusion of heat in a solid, equation (12), numerically. The equation set is very stiff, because of the highly nonlinear form of the (Arrhenius) reactions. We have therefore used a semi-implicit method to solve the equation set.

If and when the temperature rate of rise at some location suddenly "accelerates" to a value high enough that the surface glows (that is, T > 500 °C or so), we can say that smoldering ignition has occurred. The program will not tell us whether flaming ignition takes place. It also does not treat the case where the flux is applied in a crevice, such as is formed between the seat cushion and the seat back. The

program does not take into account the effect(s) of the foam possibly melting and receding away from the fabric. Finally, it also does not take oxygen diffusion within the cushion explicitly into account; hence in certain threshold situations, where a small change in oxygen concentration determines whether ignition does or does not take place, the results are ambiguous. What is and is not in the program is listed in Table 1, section II.B.

It is important to note that it is often difficult to obtain the needed kinetic and/or thermophysical parameters for the material; or, when available, to know how accurately they are known. Therefore this *caveat* must also be made: even if the program were perfect, its results are only as good as the input parameters which are supplied. On the other hand, it should accurately reproduce (or predict) trends.

There is a user-friendly front end for the input, described in Section II.C. The program runs well on a 386-level computer with a math co-processor, and faster on a 486-chip computer.

An experiment was carried out to ignite the substrate. In trying to reproduce those experimental results, it was found that the calculated results are sensitive to the input values chosen, especially the kinetic parameters. It was found that the preexponential factor found by Kashiwagi and Nambu (1992) for the oxidative pyrolysis reaction in a cellulosic paper had to be increased by 10% for the cotton duck fabric in order to get ignition for the lowest of a set of heating fluxes to which the substrate was exposed. The result was semi-quantitative agreement with the observed ignition times.

III. *CIGARET*, A MODEL OF A QUIETLY SMOLDERING, ISOLATED CIGARETTE

A. GENERAL DESCRIPTION

A cigarette consists of small strands of cured tobacco leaf (varying in length from about 0.5 to 12 mm, with the average about 3-4 mm), held in place by a paper wrapping. The shape is usually cylindrical; the radius of the cross-section is R. The circumference, $2\pi R$, generally lies between 17 and 25 mm. There is usually a filter at one end.

A schematic illustration of a smoldering cigarette in its quiescent phase is given in Figure 16. The section marked C in this figure is char, most of which is oxidizing at a rate sufficient to make it glow. The peak temperature in this region is some 800 to 850 °C; that is, about 1100 $\pm$ 25 K. The glowing coal is shaped approximately like a thick cone. The cone length varies; it is usually on the order of 1 cm.

The heat created by the char oxidation diffuses, convects *via* hot gases, and radiates away in all directions. Part of this heat is carried back towards the virgin tobacco, the zone marked VT in the figure. The tobacco just behind the burning coal then dehydrates and decomposes; this is the region marked P in the figure (P for "pyrolyzing"). This is the region from which a visible plume of smoke rises. At the front of the cigarette is the residual ash, marked A in the figure. EA stands for "evanescent ash"; that is the ash which generally falls off a cigarette, or is flicked off by the smoker. Since we will eventually assume that the cigarette rests on a substrate, the part EA might not, in fact, disappear.

We will see in Section III.C that a good deal of detail is lost when the model is assumed to be one-dimensional. Therefore the present model is two-dimensional; *i.e.*, cylindrical symmetry is assumed. This is not a bad assumption for the cigarette freely smoldering in air, but is not so good when the cigarette lies on a substrate. We nevertheless assume that whatever asymmetries are produced by that interaction can be simulated by spreading the effects of the substrate out evenly over the circumference.

B. DYNAMICS OF A SMOLDERING CIGARETTE

A good deal of effort, both experimental and theoretical, has gone into understanding the (isolated) smoldering cigarette. In this Section, a brief, qualitative discussion of the dynamical processes which occur will be presented and the salient results from earlier experiments noted. It is not intended to be an exhaustive review. For a more detailed description of cigarettes, see Gann *et al.* (1988).

1. Pyrolysis Rates

There have been many careful studies of the pyrolysis of tobacco; we will only consider some global results here. A detailed description of cigarettes can be found, for example, in Section 2 of Gann *et al.* From Table 2-3 there, it is found that for those experimental cigarettes, the average mass, exclusive of the filter, is 870 $\pm$ 470 mg. The variation for commercial cigarettes is lower. The mean mass loss rate is 60 $\pm$ 20 mg/min, corresponding, on average, to some 14 min of smolder time. This agrees with the common observation that an unattended cigarette will smolder for 10 to 20 min.

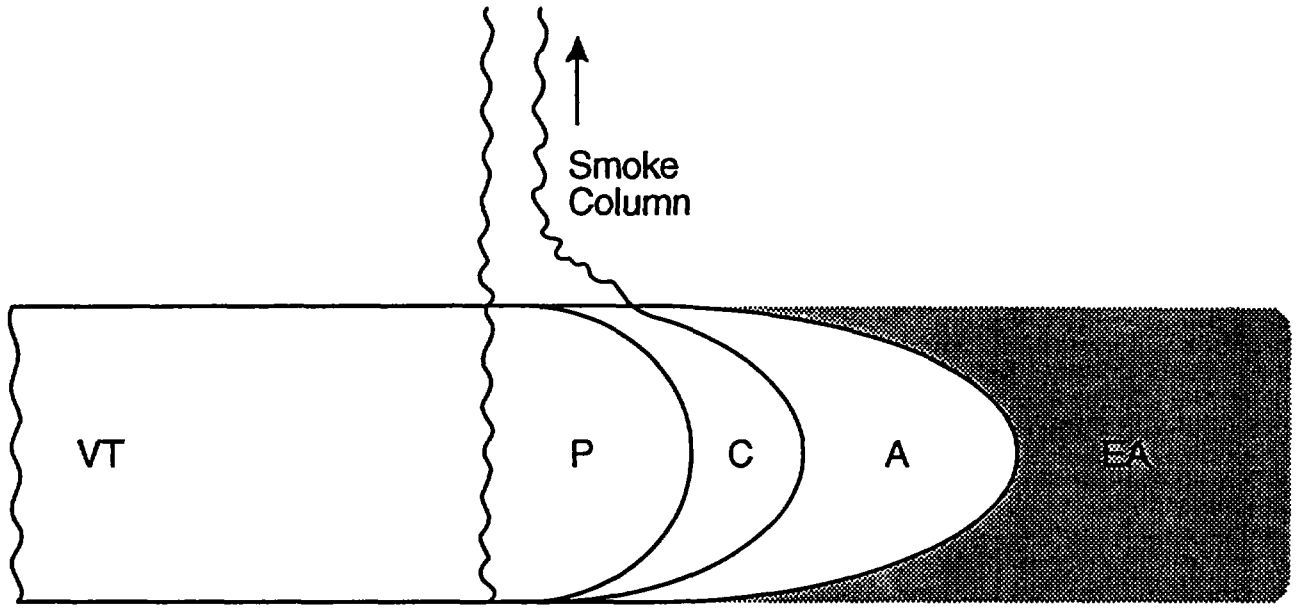

Figure 16. Schematic of a smoldering cigarette. The zone marked VT contains the virgin tobacco. P is the pyrolyzing region; the section marked C is char, A is the residual ash, and EA stands for "evanescent ash," explained in the text.

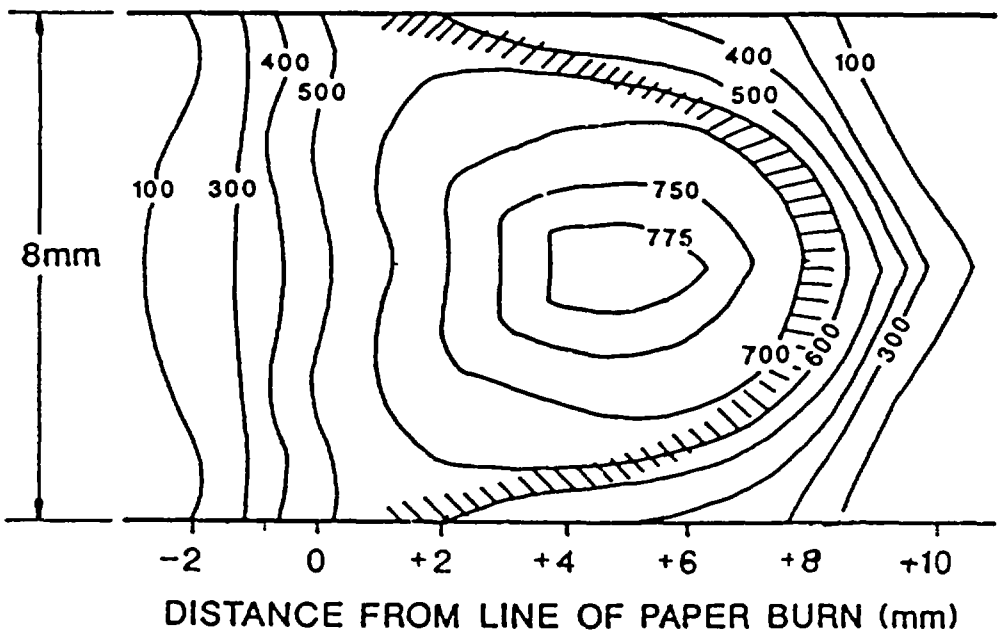

Figure 17. Isotherms in the gaseous part of the cigarette during quiet, steady burning. The shaded region indicates peak reaction rate; i.e., the glowing coal.